ACS OMEGA

Open Access

http://pubs.acs.org/journal/acsodf

Article

Optimization of 3-Cyano-7-cyclopropylamino-pyrazolo[1,5-*a*]pyrimidines toward the Development of an In Vivo Chemical Probe for CSNK2A

Xuan Yang, Han Wee Ong, Rebekah J. Dickmander, Jeffery L. Smith, Jason W. Brown, William Tao, Edcon Chang, Nathaniel J. Moorman, Alison D. Axtman, and Timothy M. Willson*

Cite This: *ACS Omega* 2023, 8, 39546−39561

Read Online

ACCESS | Metrics & More | Article Recommendations | Supporting Information

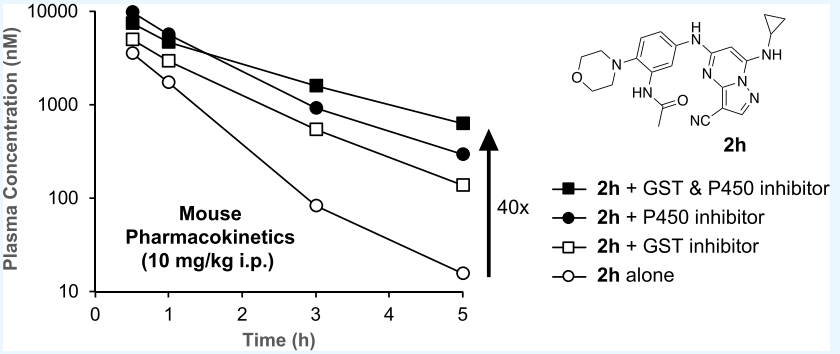

ABSTRACT: 3-Cyano-7-cyclopropylamino-pyrazolo[1,5-*a*]pyrimidines, including the chemical probe SGC-CK2-1, are potent and selective inhibitors of CSNK2A in cells but have limited utility in animal models due to their poor pharmacokinetic properties. While developing analogues with reduced intrinsic clearance and the potential for sustained exposure in mice, we discovered that phase II conjugation by GST enzymes was a major metabolic transformation in hepatocytes. A protocol for codosing with ethacrynic acid, a covalent reversible GST inhibitor, was developed to improve the exposure of analogue **2h** in mice. A double codosing protocol, using a combination of ethacrynic acid and irreversible P450 inhibitor 1-aminobenzotriazole, increased the blood level of **2h** by 40-fold at a 5 h time point.

INTRODUCTION

The appearance of a novel coronavirus SARS-CoV-2 and the resulting pandemic has highlighted the need for effective treatments against COVID-19.[1] Host-directed therapies that target cellular pathways required for virus replication have emerged as a promising approach to combat viral infections.[2] Protein kinases have been proposed as potential targets for development of antiviral drugs.[3] Among these kinases, casein kinase 2α (CSNK2A) has been shown to play a role in the replication of β-coronaviruses (β-CoV), including SARS-CoV-2.[4−6] Recent studies have demonstrated the efficacy of CSNK2A inhibitors in reducing the replication of β-CoV in vitro.[5] However, there has yet to be a demonstration of anti-COVID-19 efficacy in vivo.

3-Cyano-7-cyclopropylamino-pyrazolo[1,5-*a*]pyrimidine (PZP) is a promising chemotype of the CSNK2A inhibitor that has demonstrated potent activity in vitro.[7] PZPs possess good selectivity for CSNK2A over other kinases and display unique chemical features that contribute to their potent inhibitory activity (Figure 1). Specifically, X-ray crystallography studies (Figure 1A) revealed that the 4′-methyl substituent of the chemical probe SGC-CK2-1 (**1a**) enforces an s-cis (*E*)-conformation of the propionamide, allowing it to coordinate with a bound water molecule, which also interacts with the cyano group of the PZP core (Figure 1B). Notably, the alkyl group of the propionamide contributes to the exquisite selectivity of the PZP-based CSNK2A inhibitors over other kinases.[8] However, despite their promising in vitro activity, PZPs have shown limited bioavailability in rodents by oral dosing due to their low to moderate aqueous solubility, high first-pass metabolism, and rapid clearance.[9,10]

In this paper, we report our initial studies to identify a PZP-based CSNK2A inhibitor with potent antiviral activity and high sustained blood levels for use in a mouse-adapted model of COVID-19 developed for preclinical evaluation of potential

Received: July 24, 2023
Accepted: September 21, 2023
Published: October 10, 2023

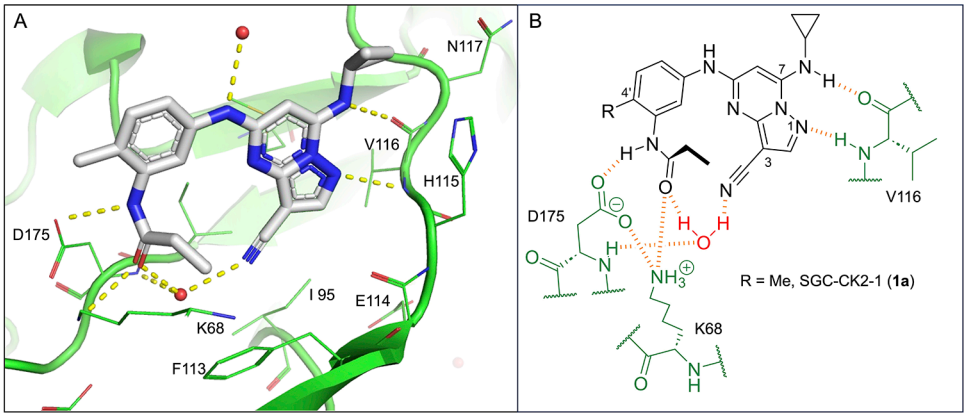

Figure 1. (A) X-ray cocrystal structure of SGC-CK2-1 (**1a**) bound to CSNK2A1 (PDB: 6Z83). Image created in PyMOL 2.4.0 with the CSNK2A1 protein shown as a green ribbon and **1a** shown as sticks colored by the atom type. Bound water molecules are shown as red spheres. Intermolecular hydrogen bonds are shown as yellow dashed lines. (B) Illustration of the key interactions observed in the X-ray structure. The 7-cyclopropylamine and N-1 of the PZP form H-bond interactions with V116 in the hinge region. The 4′-substituent (Me for **1a**) causes the amide to adopt an s-cis conformation that allows the carbonyl group to interact with K68 and a bound water molecule. The alkyl group of the amide is placed in a pocket that increases the selectivity over other kinases. The cyano group of the PZP also interacts with the bound water molecule, which is further coordinated through interaction with the backbone NH of D175.

Table 1. Modification of the 4′-Position Group of the Propionamide Series

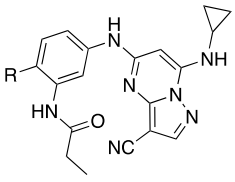

1a-i

Compound	R	CSNK2A1 pIC_{50}[a]	CSNK2A2 pIC_{50}[a]	MHV pIC_{50}[b]	cLogP[c]	Kinetic solubility (μg/mL)[d]	MLM metabolism @ 30 min (%)[e]
1a[f]	Me	7.4	7.4	6.9	0.38	1.4	60
1b[f]	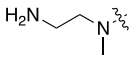	8.6	8.7	6.8	0.03	66	38
1c[f]	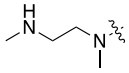	8.2	8.3	7.1	0.33	78	34
1d[f]	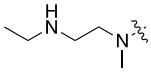	7.4	7.6	6.6	0.86	81	38
1e[f]	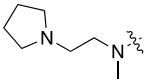	7.4	6.8	6.2	1.58	77	94
1f[f]	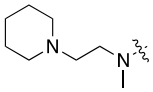	7.0	6.6	5.9	2.15	69	99
1g[f]	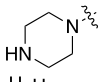	6.7	6.7	5.8	-0.03	88	12
1h	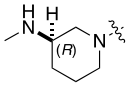	7.1	7.2	6.3	0.40	65	11
1i	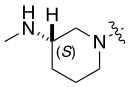	7.6	7.7	6.9	0.40	71	10

[a]In-cell target engagement by the NanoBRET assay, $n = 1$. [b]Inhibition of MHV-nLuc replication, $n = 3$ with SE ± 0.1. [c]Values from ChemDraw Professional v16.0. [d]Miniaturized shake flask using CLND detection, $n = 1$. [e]Metabolism of the compound in primary mouse liver microsomes (MLM) calculated as 100 − (% remaining), $n = 1$. [f]Compound previously reported in ref 5.

https://doi.org/10.1021/acsomega.3c05377
ACS Omega 2023, 8, 39546−39561

Scheme 1. Synthesis Previously Developed for Analogues 1b−g[a]

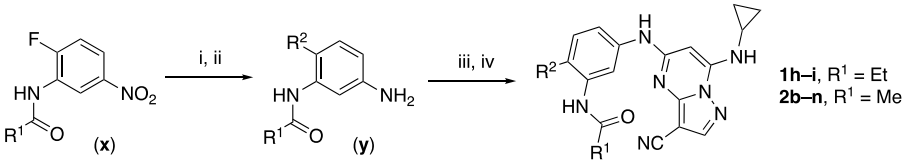

[a]Reagents and conditions: (i) R_2-H, K_2CO_3, MeCN. (ii) H_2, Pd−C, MeOH. (iii) 5-chloro-7-(cyclopropylamino)pyrazolo[1,5-*a*]pyrimidine-3-carbonitrile, BINAP, $Pd(OAc)_2$, Cs_2CO_3, dioxane, μW, 130 °C. (iv) TFA, CH_2Cl_2.

Table 2. Modification of the 4′-Position Group of the Acetamide Series

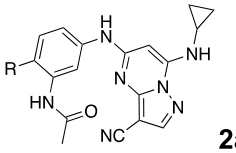

2a-n

Compound	R	CSNK2A1 pIC_{50}[a]	CSNK2A2 pIC_{50}[a]	MHV pIC_{50}[b]	cLogP[c]	Kinetic solubility (μg/mL)[d]	MLM metabolism @ 30 min (%)[e]
2a[f]	Me	9.3	9.2	7.1	-0.15	2.9	52
2b	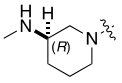	7.8	8.0	7.0	-0.13	52	14
2c	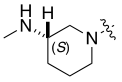	8.3	8.4	7.9	-0.13	54	14
2d	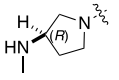	8.6	8.8	7.5	-0.69	64	8
2e	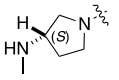	8.3	8.4	7.7	-0.69	49	16
2f	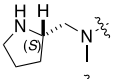	8.4	8.5	7.9	0.50	68	24
2g		7.1	7.6	5.6	-0.56	52	18
2h[f]		7.5	7.7	7.1	-0.54	1.0	30
2i	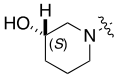	7.5	7.7	7.0	-0.50	37	55
2j		7.6	7.7	6.8	0.00	0.9	92
2k	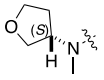	6.9	7.0	6.5	0.03	21	97
2l	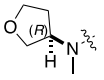	6.9	7.1	6.3	0.03	25	100
2m	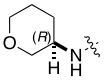	8.0	8.1	6.4	-0.23	2.4	76
2n	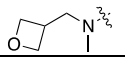	7.0	7.5	6.4	-0.70	0.2	100

[a]In-cell target engagement by the NanoBRET assay, $n = 1$. [b]Inhibition of MHV-nLuc replication, $n = 3$ with SE ± 0.1. [c]Values from ChemDraw Professional v16.0. [d]Miniaturized shake flask using CLND detection, $n = 1$. [e]Metabolism of the compound in primary mouse liver microsomes (MLM) calculated as 100 − (% remaining), $n = 1$. [f]Compound previously reported in ref 5.

drug therapies.[11,12] We discovered that the rapid clearance of PZPs in mice was due to pathways of both phase I and phase II metabolism. Codosing with a glutathione *S*-transferase (GST) enzyme inhibitor and an irreversible cytochrome P450

https://doi.org/10.1021/acsomega.3c05377
ACS Omega 2023, 8, 39546−39561

Table 3. In Vivo Mouse Pharmacokinetic Parameters of 1i, 2c, and 2e[a]

	i.v. (1 mg/kg)					i.p.(10 mg/kg)			
compound	C_{max} (ng/mL)	AUC_{last} (ng·h/mL)	Vd_{ss} (L/kg)	$t_{1/2}$ (h)	CL_{int} (mL/min/kg)	C_{max} (ng/mL)	AUC_{last} (ng·h/mL)	$t_{1/2}$ (h)	F (%)
1i	1100	670	2.60	1.3	36	4700	7010	1.2	100
2c	350	200	5.07	1.8	84	670	770	1.5	40
2e	810	250	2.67	1.2	69	1500	1300	1.4	53

[a]Mice dosed by i.v. or i.p. route of administration, n = 3. Compounds quantified by LC-MS.

inhibitor greatly reduced the intrinsic clearance of a PZP analogue in mice and may be a viable approach to increase in vivo exposure for preclinical pharmacology studies.

RESULTS

Antiviral PZPs with Reduced Phase I Metabolism. All compounds were screened for CSNK2A1 and CSNK2A2 activity using a NanoBRET assay in HEK293 cells and for inhibition of mouse β-CoV replication using an MHV-nLuc assay in DBT cells.[5] Kinetic solubility was determined by using a miniaturized shake flask method. The stability of compounds to phase I metabolism was determined by incubation with mouse liver microsomes for 30 min. SGC-CK2-1 (**1a**) demonstrated low aqueous solubility and rapid metabolism in primary mouse liver microsomes (MLM), with only 40% of the parent compound remaining after 30 min (Table 1). Since hepatic metabolism of **1a** would likely lead to rapid in vivo clearance, we decided to focus initially on increasing its stability in MLM. SMARTCyp,[13,14] a web-based predictor of metabolic hot spots, analyzes sites of metabolism using a ligand-based approach from a library of molecular fragments that can be applied across multiple species and isoforms of CYPs.[15] SMARTCyp suggested that the cyclopropylamine and the 4′-methyl group might be sites of P450 oxidation (Figure S1). As modification of the cyclopropylamine, which forms part of the hinge-binding motif (Figure 1B), resulted in a large decrease in CSNK2A potency,[5,8] we opted to study analogues with modification of the 4′-methyl group to lower log$D$, improve aqueous solubility, and possibly reduce P450 metabolism.[16] Analogues **1b**−**g** with substituted ethylenediamines replacing the 4′-methyl group demonstrated good CSNK2A potency and retained antiviral activity, as previously reported.[5] Analogues **1b**−**g** had around 50- to 60-fold improved aqueous solubility. The ethylenediamines **1b**−**d** also had reduced metabolism in MLM compared to that of **1a** (Table 1). In contrast, diamines containing a pyrrolidine (**1e**) or piperidine (**1f**) were highly metabolized despite their improved aqueous solubility, possibly due to their increased lipophilicity. The piperazine (**1g**) had greatly improved metabolic stability but at a cost of lower CSNK2A potency and antiviral IC_{50} > 1 μM. From this initial series of analogues of **1a**, we found that the addition of ethylenediamines at the 4′-position resulted in PZPs with good antiviral activity and reduced P450 metabolism in MLM. Although the piperazine **1g** had the best metabolic stability, it showed reduced potency in both CSNK2A and antiviral assays.

To build on these results, we designed new analogues with 3-aminomethylpiperidine substituents at the 4′-position to combine the features of both the cyclic and linear diamines. The synthesis employed the methods previously developed for analogues **1b**−**g** (Scheme 1). Addition of the (*R*)- or (*S*)-enantiomer of the *N*-Boc-protected 3-aminomethylpiperidine to the acyl-2-fluoro-5-nitroaniline (**x**, R^1 = Et) followed by reduction of the nitro group yielded the aniline intermediate (**y**, R^1 = Et). Palladium-catalyzed Buchwald−Hartwig cross-coupling with the 5-chloro-pyrazolo[1,5-*a*]pyrimidine core followed by *N*-Boc deprotection yielded the 3*R*-isomer (**1h**) and the 3*S*-isomer (**1i**). Both isomers, **1h** and **1i**, demonstrated good aqueous solubility and low metabolism in mouse liver microsomes compared to **1a** (Table 1). The 3*S*-isomer (**1i**) was more potent than the 3*R*-isomer (**1h**) in both the CSNK2A and antiviral assay. Overall, **1i** had a comparable potency to **1a** but with improved solubility and metabolic stability.

To further improve the potency, we synthesized 4′-substituted analogues in the acetamide series of PZPs (Table 2). The compounds were synthesized by the established route from the acyl-2-fluoro-5-nitroaniline (**x**, R^1 = Me) and the appropriate secondary amine for the R^2-substituent (Scheme 1). For those R^2-substituents with chiral centers, the enantiomerically pure amine was utilized as a building block. The 4′-methyl analogue (**2a**) had shown subnanomolar activity on CSNK2A and good activity in the antiviral assay.[5] **2a** had a lower clog$P$ and slightly improved solubility and metabolic stability compared to the corresponding propionamide (**1a**) (Table 2). The synthesis of the 3*R*-isomer (**2b**) and 3*S*-isomer (**2c**) of the 3-aminomethylpiperidine gave analogues with 10-fold improved potency in the CSNK2A and the antiviral assays while maintaining good metabolic stability. The 3*S*-isomer (**2c**) was again the more potent of the two enantiomers. Additional 4′-substituted analogues were synthesized in the acetamide series. The 3*R*-isomer (**2d**) and 3*S*-isomer (**2e**) of the 3-aminomethyl pyrrolidine also combined potency on CSNK2A and antiviral activity with good metabolic stability. Switching the orientation of the 3-aminomethyl pyrrolidine gave analogue **2f** with similar potency but slightly poorer metabolic stability. The piperazine (**2g**) was less potent on CSNK2A and in the antiviral assay, but had good metabolic stability, as had been seen in the corresponding propionamide (**1g**). We had previously prepared and tested morpholine (**2h**),[5] which had improved antiviral activity compared to **2g**. Although morpholine (**2h**) showed low aqueous solubility, its metabolic stability was much better than the parent analogue **2a** (Table 2). The introduction of a hydroxy substituent in **2i** maintained activity and improved aqueous solubility but decreased the metabolic stability. The oxo-analogues **2j**−**n** had lower activity in the antiviral assay and poor metabolic stability, despite some analogues (e.g., **2l**) having low clog$P$ and good solubility.

Pharmacokinetic Profiling of PZPs. Having identified several analogues with improved metabolic stability in MLM and potent activity in the CSNK2A and antiviral assays, we selected three compounds (**1i**, **2c**, and **2e**) for pharmacokinetic studies. These analogues showed only 10−16% metabolism in the primary MLM after 30 min of incubation. The compounds were dosed at 1.0 mg/kg i.v. and 10 mg/kg i.p. to mice, and the level of the parent compound was monitored over 24 h (Table

https://doi.org/10.1021/acsomega.3c05377
ACS Omega 2023, 8, 39546−39561

3). Despite their stability in MLM, all three compounds demonstrated moderate to high clearance following i.v. dosing, with a $t_{1/2}$ of 1.2−1.8 h. Similar results were observed following i.p. dosing with a $t_{1/2}$ of 1.2−1.5 h. Although the bioavailability by i.p. dosing was good, the rapid clearance resulted in low total exposure and blood levels that fell below the IC_{50} for antiviral activity within 1 h.

Phase II Metabolism of PZPs. To further explore the reason for the rapid in vivo clearance of the PZPs (**1i**, **2c**, and **2e**), we performed time course studies to measure their rate of intrinsic clearance using in vitro systems of hepatic metabolism (Table 4). In mouse primary liver microsomes, the three compounds showed low intrinsic clearance consistent with the single time point measurements (Tables 1 and 2). Repeating the experiment with primary liver microsomes that included the S9 fraction resulted in a decrease in clearance, indicating that metabolic stability was unaffected by the inclusion of the cytosolic enzymes. However, when incubated with primary mouse hepatocytes, all three compounds were rapidly metabolized with high rates of intrinsic clearance (Table 4). The results suggested that a non-P450 metabolic pathway could be responsible for the rapid hepatic clearance of the PZPs in hepatocytes and in mice in vivo.[17]

Table 4. In Vitro Mouse Metabolism of 1i, 2c, and 2e[a]

compound	liver microsomes CL_{int} (mL/min/kg)	S9 fraction CL_{int} (mL/min/kg)	hepatocytes CL_{int} (mL/min/kg)
1i	<24	0	143
2c	<24	1	132
2e	27	4	69

[a]Compounds quantified by LC-MS at five time points over 5 h, $n = 1$.

Metabolite ID Study of 1i. To identify the metabolic pathway responsible for the rapid clearance in mouse hepatocytes, we performed a metabolite ID study using 3*S*-aminomethylpiperidine (**1i**). Incubation of **1i** for 4 h in primary cultures of mouse hepatocytes resulted in the appearance of 12 metabolites with unique retention times by ultrahigh performance liquid chromatography (uHPLC) (Figure 2A). Analysis of the metabolites by mass spectroscopy and quantification by UV absorbance enabled the assignment of the primary pathways of metabolic transformation (Table 4 and Figure 2B and Figure S2). Six metabolites (M1−M5 and M10) were assigned structures that resulted from GSH conjugation of the PZP (Figure 2B), a phase II metabolic transformation that could only occur in whole hepatocytes that contain active GST enzymes. GSH conjugation was observed in the major fraction of the total metabolites, as quantified by UV absorbance (Table 5) and is likely to be an important pathway of clearance of the PZP **1i** (Figure 2B). A trio of GSH conjugates, M3, M4, and M5, were observed with the same molecular weight but different uHPLC retention times. They were assigned as constitutional isomers, resulting from GSH conjugation at different positions of the PZP (Figure 2B). Another pair of metabolites, M1 and M2, that arise from an additional oxidative dealkylation of the cyclopropyl group are also constitutional isomers from the conjugation of GSH at different positions on the PZP. M10 was a unique metabolite from cleavage of the bond between the piperidine and the phenyl ring in addition to GSH conjugation. Demethylation of the secondary amine on the piperidine was found in M6 and M11 as the other main site of metabolism (Table 4 and Figure 2B). Several minor pathways of oxidation, amide hydrolysis, and dehydrogenation were also assigned by analysis of the metabolites M7−M9 and M12 (Figure 2B). The initial P450 oxidation of electron-rich aromatic rings to arene oxide[18] or quinone−imine[19] intermediates are known activation steps for GSH conjugation, making the amino-substituted phenyl ring the most likely site of phase II metabolism (Figure 2C). Although we initially considered the nitrile as a potential site of conjugation, since it can undergo a Pinner reaction with free GSH,[20] there is no evidence that the reaction is catalyzed by GST enzymes.[21,22] Thus, the metabolite ID study implicated both cytochrome P450 and GST enzymes as likely to be responsible for the rapid clearance of the PZPs in mouse hepatocytes through a combination of demethylation and GSH conjugation (Figure 2C).

Hepatocyte Metabolism of Antiviral PZPs. Eight acetamide PZPs (**2a−f** and **2h−i**) with an $IC_{50} \leq 100$ nM in the antiviral assay were selected for time course metabolic stability profiling in mouse and human primary hepatocytes (Table 6). Unfortunately, all acetamide PZPs (**2a−f** and **2h−i**) showed high intrinsic clearance in mouse hepatocytes, independent of their stability in liver microsomes (Table 2), suggesting that they were substrates for phase II GST enzymes. The in vitro metabolism data in mouse hepatocytes predicted that acetamide PZPs with potent antiviral activity would likely have a rapid in vivo clearance in mice. In contrast, the compounds had much lower intrinsic clearance in human primary hepatocytes, with only **2h** and **2i** showing moderate and high rates of clearance, respectively. These results demonstrated that the metabolism of the PZPs in primary hepatocytes was predominantly a species-specific issue, with intrinsic clearance always much higher in mouse than human hepatocytes. Although this was a promising result for the future development of PZPs as therapeutic drugs for use in humans, it still limited their utility as pharmacological tools for studies in mice.

Inhibition of GSH Conjugation in Hepatocytes. Given our primary objective of identifying a potent CSNK2A inhibitor for use in an in vivo mouse COVID-19 efficacy model to validate the host kinase as a potential antiviral drug target, we opted to explore the effect of inhibition of phase II GST enzymes on intrinsic clearance. Ethacrynic acid (EA) is an FDA-approved loop diuretic that is also a potent covalent, but reversible, inhibitor of GST enzymes.[23] EA has demonstrated potent inhibition of GST enzymes in a perfused rat liver and human cancer cell lines,[23] and although it has been used in human clinical studies to block GSH conjugation,[24] there are only a few reports of its use in rodents as a GST inhibitor.[25−27] To determine if EA could improve the metabolic stability of a PZP in primary mouse hepatocytes, we tested the effect of codosing on the stability of **2h**, which was one of the analogues with the highest intrinsic clearance (Table 6). The intrinsic clearance of **2h** in primary mouse hepatocytes was determined by measuring the decrease in the level of the parent compound over 2 h (Figure 3). Parallel sets of incubations were performed in the presence of increasing doses of EA from 0 to 400 μM. Intrinsic clearance was >250 mL/min/kg in the absence of EA. However, in the presence of doses of EA from 10 to 50 μM, the intrinsic clearance was decreased by >50% (Figure 3). At doses of EA above 100 μM, the intrinsic clearance of **2h** was further decreased to <50 mL/min/kg. These codosing experiments in primary mouse hepatocytes demonstrated that EA was

https://doi.org/10.1021/acsomega.3c05377
ACS Omega 2023, 8, 39546−39561

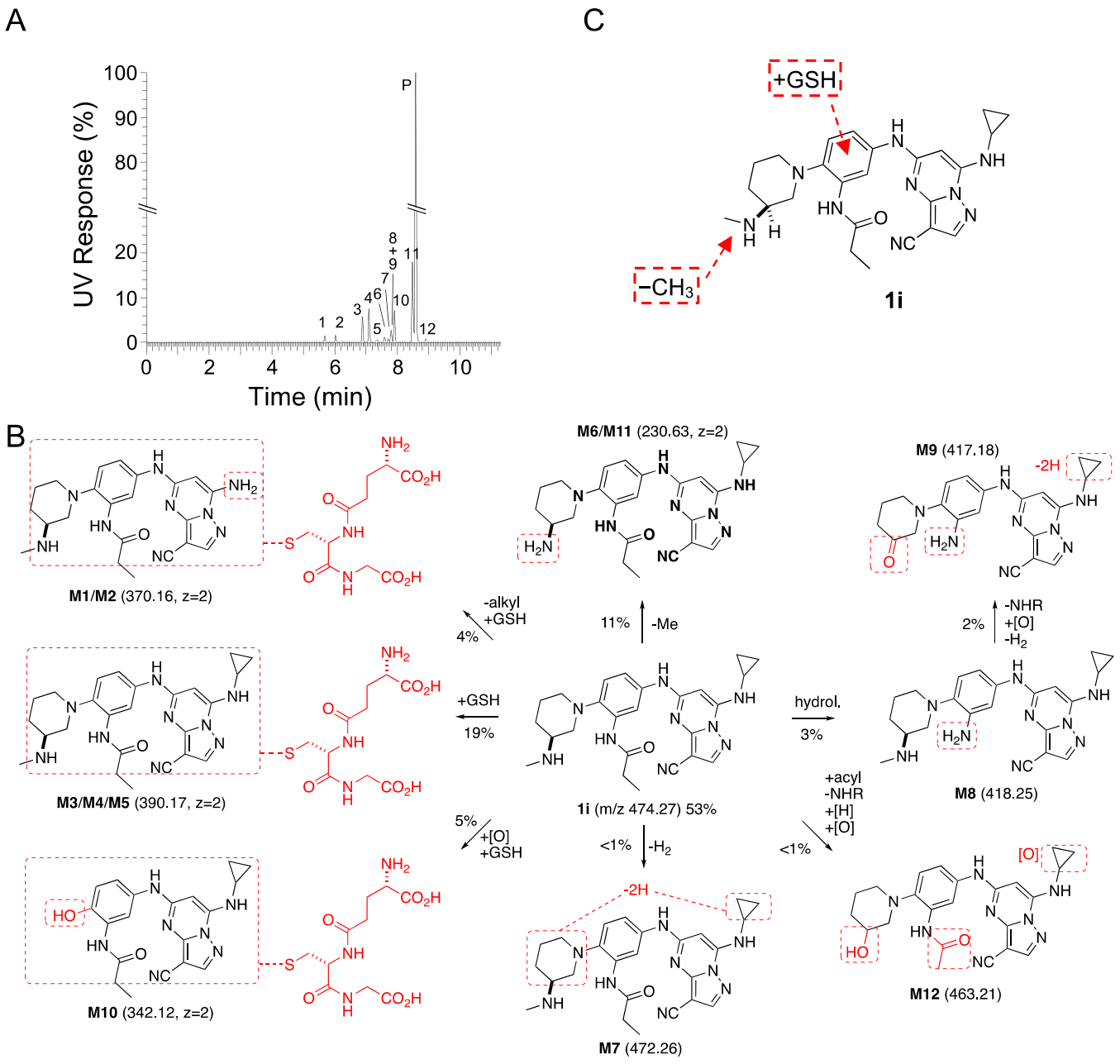

Figure 2. (A) Identification of 12 metabolites of **1i** (parent P) after incubation in mouse primary hepatocytes for 4 h. The relative quantity of each metabolite was determined by UV. (B) Structural assignment of the metabolites (M1−M12) from MS fragmentation (see Figure S2). Molecular ions are shown in parentheses. Doubly charged ions are indicated as $z = 2$. The relative percent contribution of each metabolite taken from Table 5. (C) Summary of the major sites of metabolism of **1i** in mouse primary hepatocytes.

effective at increasing the metabolic stability of PZP **2h**, presumably by blocking its GSH conjugation.

Codosing of 2h with Inhibitors of Metabolic Enzymes In Vivo. To determine if inhibition of GSH conjugation could be an effective strategy to increase the bioavailability of **2h** in vivo, we performed a series of codosing studies in mice of **2h** with either EA or 1-aminobenzotriaole (1-ABT), a widely used broad-spectrum inhibitor of mouse cytochrome P450s[28] (Figure 4). When dosed alone to mice at 10 mg/kg i.p., **2h** was rapidly cleared from the circulation with $t_{1/2}$ = 35 min and AUC of around 4000 h·nM. A 6 h pretreatment and codosing with 10 mg/kg i.p. EA resulted in a small increase in $t_{1/2}$ and AUC. Increasing the dose to 30 mg/kg i.p. EA resulted in an additional increase in both parameters, demonstrating that the inhibition of GST enzymes could reduce the intrinsic clearance of **2h**. The 30 mg/kg i.p. dose of EA increased the $t_{1/2}$ by 1.5-fold and AUC by 1.8-fold. Unfortunately, we were unable to further increase the dose of EA to 100 mg/kg i.p. due to the observation of toxicity in mice on repeated dosing (Table S1). Since GSH conjugation of electron-rich aromatic groups requires an initial cytochrome P450 oxidation step, we also evaluated the in vivo pharmacokinetics of **2h** in mice pretreated with 1-ABT for 2 h. 1-ABT was able to reduce the CL_{int} of **2h** in primary mouse hepatocytes to <32 mL/min/kg (Figure S3). A decrease in the clearance of **2h** was also observed in mice treated with 1-ABT at 100 mg/kg p.o. with increases in $t_{1/2}$ and AUC of 1.6- and 3.5-fold, respectively, compared to the dosing of **2h** alone. The larger increase in

https://doi.org/10.1021/acsomega.3c05377
ACS Omega 2023, 8, 39546−39561

Table 5. Metabolites of 1i in Mouse Hepatocytes

			transformation									
peak[a]	time (min)	mass (m/z)	−alkyl	+GSH	$-CH_3$	$-H_2$	hydrol.	$-NH_2$	[O]	[H]	acyl.	rel. (%)
M1	5.67	370.16[b]	X	X								<1
M2	6.03	370.16[b]	X	X								3
M3	6.89	390.17[b]		X								9
M4	7.10	390.17[b]		X								9
M5	7.34	390.17[b]		X								<1
M6	7.59	230.63[b]			X							<1
M7	7.70	472.26				X						<1
M8	7.79	418.25					X					<1
M9	7.80	417.18				X	X	X	X			2
M10	7.91	342.12[b]		X					X			5
M11	8.47	230.63[b]			X							10
parent	8.58	474.27										53
M12	8.90	463.21					X	X	X	X	X	<1
total rel. (%)[c]			4	27	11	3	4	3	8	1	1	

[a]See Figure 2 for structural assignments. [b]$[M + 2H]^{2+}$, $z = 2$. [c]Sum of metabolites with the transformation, using <1 = 1.

Table 6. Mouse and Human Hepatocyte Clearance[a]

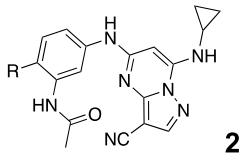

2

Compound	R	Mouse Hepatocyte CL_{int} (mL/min/kg)	Human Hepatocyte CL_{int} (mL/min/kg)
2a	Me	173	8
2b	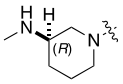	162	0
2c	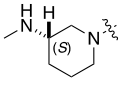	132	0
2d	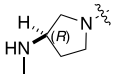	126	0
2e	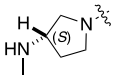	69	0
2f	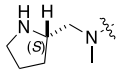	171	0.8
2h		279	23
2i	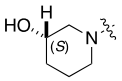	511	73

[a]Compounds quantified by LC-MS at five time points over 5 h, $n = 1$.

AUC with 1-ABT compared with EA may be due to the direct inhibition of phase I P450 metabolism and indirect inhibition of phase II GSH conjugation. Importantly, the results demonstrated that it was possible to increase the circulating levels of the PZP CSNK2A inhibitor **2h** by codosing with either a GST inhibitor or a P450 inhibitor. Finally, to determine whether combined codosing with EA and 1-ABT could further decrease the clearance of **2h**, we performed a study in the presence of both the GST and P450 inhibitors. A combination of 30 mg/kg i.p. EA (6 h pretreatment and codosed) with 100 mg/kg p.o. 1-ABT (2 h pretreatment) resulted in the highest levels of **2h** at the 3 and 5 h time points (Figure 4), with the $t_{1/2}$ increased by 2.4-fold compared to dosing of **2h** alone.

https://doi.org/10.1021/acsomega.3c05377
ACS Omega 2023, 8, 39546−39561

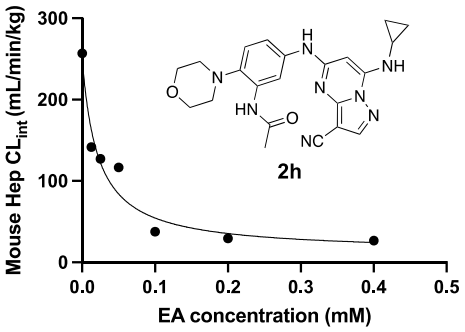

Figure 3. Mouse hepatocyte clearance of **2h** in the presence of GST inhibitor EA.

A

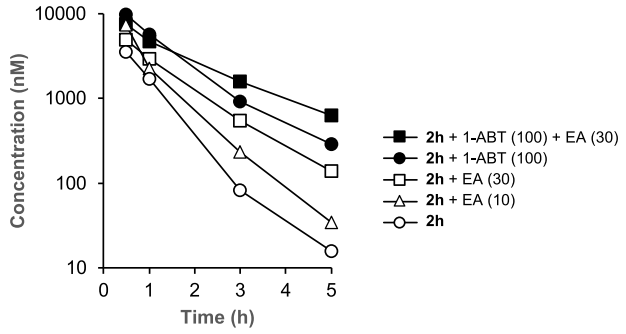

B

	2h i.p. (10)				
		+EA (10)	+EA (30)	+1-ABT (100)	+EA (30) +1-ABT (100)
$t_{1/2}$ (h)	0.59	0.66	0.90	0.93	1.4
C_{max} (nM)	3520	7350	4970	9730	7500
AUC_{last} (h*nM)	4090	7010	7410	14100	13400

Figure 4. In vivo clearance of **2h** in mice in the presence of a GST inhibitor (EA) or a P450 inhibitor (1-ABT). (A) Blood levels of **2h** over 5 h following a 10 mg/kg dose i.p. All data are the average from three mice. The dose of EA or 1-ABT is indicated in parentheses in mg/kg. EA was administered i.p. as a 6 h pretreatment and again codosed with **2h**. 1-ABT was administered p.o. as a 2 h pretreatment. (B) Pharmacokinetic parameters.

DISCUSSION AND CONCLUSIONS

The 3-cyano-7-cyclopropylamino-pyrazolo[1,5-*a*]pyrimidine (PZP) is the most potent and selective chemotype of ATP-competitive CSNK2A inhibitors,[7] with fewer kinase off-targets than silmitasertib and related compounds.[29] SGC-CK2-1 (**1a**)[8] has been established as a high-quality chemical probe for studying CSNK2 signaling in the phenotypic assay and human-derived primary cells.[30−32] However, the use of PZP-based CSNK2A inhibitors as chemical probes in rodent pharmacology models has been limited by their generally poor pharmacokinetic properties. Although Dowling and co-workers reported that **2a** had modest oral bioavailability in rats (10 mg/kg, C_{max} = 300 nM, F = 25%), it showed in vivo activity only at short time points after dosing.[9] After extensive work on the series, Dowling and co-workers concluded that an analogue with an ethylenediamine substituent at the 4′-position could be used as a pharmacological tool by i.v. or i.p. dosing, despite its rapid clearance in rats.[10] For the studies reported herein, we decided to focus on development of an in vivo pharmacological probe that would maintain high sustained exposure in mice following i.p. dosing since this route of administration was preferred in many academic laboratories for preclinical target validation studies.[33]

Initially, we examined the potential of the 4′-substitued analogues of SGC-CK2-1 (**1a**) to improve solubility and reduce its rapid metabolism in mouse liver microsomes. Testing several of the previously prepared analogues of **1a**[5,8] confirmed prior observations[10] of reduced metabolism of linear and cyclic diamine analogues with clog$P$ < 0.5 (Table 1). After synthesizing many new 4′-substituted PZPs in the acetamide (**1**) and propionamide (**2**) series, the chiral 3-methylamino-pipiperides **1h−i** and **2b−c** and 3-methylaminopyrollidines **2d−e** were found to have the best balance of reduced MLM metabolism and good cellular potency in the antiviral assay. However, despite their improved stability to phase I metabolism, **1i**, **2c**, and **2e** showed rapid clearance in mice following i.v. or i.p. administration (Table 3).

After discovering that **1i**, although stable in MLM, was rapidly metabolized in mouse primary hepatocytes, we performed a metabolic ID study that identified phase II GSH conjugation as a major metabolic transformation (Table 4 and Figure 2). This result suggested that phase II metabolism by GST enzymes was a previously underappreciated metabolic liability of PZPs containing electron-rich di- and tri-aniline rings. Unfortunately, all potent antiviral PZPs showed rapid metabolism in mouse primary hepatocytes (Table 6). Although the metabolic instability may be species-specific, since it was not observed in human primary hepatocytes, the rapid clearance in mouse primary hepatocytes predicted that none of the potent antiviral PZP analogues would be suitable for use in the mouse-adapted COVID-19 model.

To explore ways to reduce the phase II metabolism of a PZP analogue, we investigated codosing with EA, a well-characterized broad-spectrum covalent, but reversible, inhibitor of rodent and human GSTs.[23] The studies were performed with the morpholine analogue **2h**, which exhibited potent antiviral activity but very high clearance in primary mouse hepatocytes. Codosing of EA with **2h** in primary mouse hepatocytes demonstrated that metabolism could be reduced in a dose-dependent manner, with >90% reduction in intrinsic clearance at EA concentrations >100 μM (Figure 3).

Translating the use of EA as a GST inhibitor to an in vivo setting in mice was not straightforward. EA is an inhibitor of NKCC2, a Na−K−Cl transporter, and is approved for use in humans as a loop diuretic for treatment of high blood pressure and edema.[34] At its commonly used 50 mg oral dose in humans, EA does not cause significant drug−drug interactions that might result from GST inhibition. However, in rodents, no dose-ranging studies to establish the lowest effective dose for GST inhibition have been reported. Although, doses of 10−20 mg/kg p.o. have been used to boost the activity of oncology drugs in mice.[25−27] Our pharmacokinetic studies in mice revealed that the maximum tolerated dose of EA by i.p. dosing was only 30 mg/kg. Doses of 100 mg/kg and higher resulted in clinical symptoms including death (Table S1). Although the reason for the toxicity of EA by i.p. administration is unclear, the rapid onset suggests that it may be unrelated to the inhibition of liver metabolism enzymes. Nevertheless, we observed a reduction in the plasma clearance of **2h** in mice at both the 10 and 30 mg/kg i.p. codoses of EA without toxicity. Furthermore, the clearance of **2h** was also reduced by a 100 mg/kg p.o. dose of the irreversible cytochrome P450 inhibitor 1-ABT, which would be expected to block directly phase I metabolism as well as indirectly phase II metabolism that

https://doi.org/10.1021/acsomega.3c05377
ACS Omega 2023, 8, 39546−39561

proceeds through arene oxide or quinone−imine intermediates. The most effective strategy to decrease the clearance of **2h** was a codosing protocol, using a combination of 30 mg/kg i.p. EA and 100 mg/kg p.o. 1-ABT. With this approach, the blood level of **2h** was boosted 40-fold at the 5 h time point.

In conclusion, our findings demonstrate that phase II metabolism limits the in vivo exposure of PZP-based CSNK2A inhibitors in mice and severely limits their utility as pharmacological probes despite their remarkable potency and selectivity in cells. Although the use of EA as a GST inhibitor provides an effective method to reduce the intrinsic clearance of the current antiviral PZP molecules in mice, we are continuing to optimize the series to identify new analogues with reduced potential for phase II metabolism. Our goal is to find in vivo chemical probes for CSNK2A that can be dosed in mice without the additional complication of codosing with multiple inhibitors of drug-metabolizing enzymes.

EXPERIMENTAL SECTION

NanoBRET Assay. Assays were run with a modified version of the previously published protocols.[5,8] HEK293 cells were cultured at 37 °C in 5% CO_2 in Dulbecco's modified Eagle medium (DMEM; Gibco) supplemented with 10% fetal bovine serum (VWR/Avantor). A transfection complex of DNA at 10 μg/mL was created, consisting of 9 μg/mL carrier DNA (Promega) and 1 μg/mL CSNK2A-NLuc fusion DNA in Opti-MEM without serum (Gibco). FuGENE HD (Promega) was added at 30 μL/mL to form a lipid:DNA complex. The solution was then mixed and incubated at room temperature for 20 min. The transition complex was mixed with a 20× volume of HEK293 cells at 20,000 cells/mL in DMEM/FBS, and 100 μL/well was added to a 96-well plate that was incubated overnight at 37 °C and 5% CO_2. The following day, the media were removed via aspiration and replaced with 85 μL of Opti-MEM without phenol red. A total of 5 μL per well of 20× NanoBRET Tracer K10 (Promega) at 10 μM for CSNK2A1 or 5 μM for CSNK2A2 in Tracer Dilution Buffer (Promega N291B) was added to all wells, except the "no tracer" control wells. Test compounds (10 mM in DMSO) were diluted 100× in Opti-MEM media to prepare stock solutions and evaluated at 11 concentrations. A total of 10 μL per well of the 10-fold test compound stock solutions (final assay concentration of 0.1% DMSO) were added. For "no compound" and "no tracer" control wells, DMSO in Opti-MEM was added for a final concentration of 1.1% across all wells; 96-well plates containing cells with NanoBRET Tracer K10 and test compounds (100 μL total volume per well) were equilibrated (37 °C/5% CO_2) for 2 h. The plates were cooled to room temperature for 15 min. The NanoBRET NanoGlo substrate (Promega) at a ratio of 1:166 to Opti-MEM media in combination with an extracellular NLuc Inhibitor (Promega) diluted at 1:500 (10 μL of 30 mM stock per 5 mL of the Opti-MEM plus substrate) was combined to create a 3× stock solution. A total of 50 μL of the 3× substrate/extracellular NL inhibitor was added to each well. The plates were read within 30 min on a GloMax Discover luminometer (Promega) equipped with a 450 nm BP filter (donor) and 600 nm LP filter (acceptor) using 0.3 s of integration time. Raw milliBRET (mBRET) values were obtained by dividing the acceptor emission values (600 nm) by the donor emission values (450 nm) and multiplying by 1000. Averaged control values were used to represent complete inhibition (no tracer control: Opti-MEM + DMSO only) and no inhibition (tracer only control: no compound, Opti-MEM + DMSO + Tracer K10 only) and were plotted alongside the raw mBRET values. The data was first normalized and then fit using the Sigmoidal 4PL binding curve in Prism Software to determine IC_{50} values.

MHV Assay. DBT cells were cultured at 37 °C in Dulbecco's modified Eagle medium (DMEM; Sigma-Aldrich) supplemented with 10% fetal bovine serum (Gibco) and penicillin and streptomycin (Sigma-Aldrich). DBT cells were plated in 96-well plates to be 80% confluent at the start of the assay. Test compounds were diluted to 15 μM in DMEM. Serial 4-fold dilutions were made in DMEM, providing a concentration range of 15−0.22 μM. Media were aspirated from the DBT cells, and 100 μL of the diluted test compounds was added to the cells for 1 h at 37 °C. After 1 h, MHV-nLuc[5] was added at an MOI of 0.1 in 50 μL of DMEM so that the final concentration of the first dilution of the compound was 10 μM (T = 0). After 10 h, the media were aspirated, and the cells were washed with PBS and lysed with passive lysis buffer (Promega) for 20 min at room temperature. Relative light units (RLUs) were measured by using a luminometer (Promega; GloMax). Triplicate data was analyzed in Prism Graphpad to generate IC_{50} values.

Kinetic Solubility. Phosphate buffered saline (50 mL, PBS, Fisher, pH 7.4) was added to HPLC grade H_2O (450 mL) for a total dilution factor of 1:10 and final PBS concentration of 1×. The test compound (6 μL) as a 10 mM DMSO stock solution was combined with the aqueous PBS solution (294 μL) for 50-fold dilution in a Millipore solubility filter plate with a 0.45 μM polycarbonate filter membrane using a Hamilton Starlet liquid handler. The final DMSO concentration was 2.0%, and the maximum theoretical compound concentration was 200 μM. The filter plate was heat-sealed for the duration of a 24 h incubation period. The sample was placed on a rotary shaker (200 rpm) for 24 h at ambient temperature (21.6−22.8 °C) and then vacuum-filtered. All filtrates were injected into a chemiluminescent nitrogen detector for quantification. The equimolar nitrogen response of the detector was calibrated using standards that span the dynamic range of the instrument from 0.08 to 4500 μg/mL nitrogen. The filtrates were quantified with respect to this calibration curve. The calculated solubility values were corrected for background nitrogen present in DMSO and the media used to prepare the samples.

Mouse Liver Microsomal Stability. Compounds as 10 mM DMSO stock solutions were diluted to 2.5 mM with DMSO and again to 0.5 mM with MeCN to give a final solution containing a 0.5 mM compound in 1:4 DMSO/MeCN. Liver microsomes from male CD-1 mice were sourced from Xenotech (Kansas City, KS), lot no. 1710069. A reaction plate was prepared by adding 691.25 μL and prewarmed (37 °C) microsomal solution (0.63 mg/mL protein in 100 mM KPO_4 with 1.3 mM EDTA) to an empty well of a 96-well plate and maintained at 37 °C. The diluted 0.5 mM compound (8.75 μL) was added to the microsomal solution in the reaction plate and mixed thoroughly by repeated pipetting to give a final assay concentration of the 5.0 μM compound. The resulting solutions were preincubated for 5 min at 37 °C and then dispensed into T = 0 and incubation plates. For the T = 0 plates, an aliquot (160 μL) of each reaction solution was added to an empty well of a 96-well plate as an exact replicate of the reaction plate. Cold (4 °C) MeOH (400 μL) was added to each well and mixed thoroughly by repeated pipetting. NADPH regeneration solution (40 μL) was added to each well and mixed thoroughly by repeated pipetting. For the T =

https://doi.org/10.1021/acsomega.3c05377
ACS Omega 2023, 8, 39546−39561

30 min incubation plate, NADPH (95 μL) was added to the remaining solution (microsomes + test compound) in each well in the previously prepared reaction plate to initiate the reaction. The plate was sealed and incubated at 37 °C for 30 min. An aliquot (100 μL) was removed from each well at the desired time point and dispensed into a well of a 96-well plate. Cold (4 °C, 200 μL) MeOH was added to quench the reaction. All plates were sealed, vortexed, and centrifuged at 3000 rpm, 4 °C for 15 min, and the supernatants were transferred for analysis by LC-TOFMS. The supernatant (20 μL) was injected onto an AQUASIL C18 column and eluted using a fast-generic gradient program. TOFMS data was acquired using Agilent 6538 Ultra High Accuracy TOF MS in extended dynamic range (m/z 100−1000) using generic MS conditions in positive mode. Following data acquisition, exact mass extraction and peak integration were performed using MassHunter Software (Agilent Technologies). The stability of the compound was calculated as the percent remaining of the unchanged parent at T = 30 min relative to the peak area at T = 0 min.

To determine CL_{int}, aliquots of 50 μL were taken from the reaction solution at 0, 15, 30, 45, and 60 min. The reaction was stopped by the addition of four volumes of cold MeCN with IS (100 nM alprazolam, 200 nM imipramine, 200 nM labetalol, and 2 μM ketoprofen). Samples were centrifuged at 3,220g for 40 min, and 90 μL of the supernatant was mixed with 90 μL of ultrapure H_2O and then used for LC-MS/MS analysis. Peak areas were determined from extracted ion chromatograms, and the slope value, k, was determined by linear regression of the natural logarithm of the remaining percentage of the parent drug vs incubation time curve. The intrinsic clearance (CL_{int} in μL/min/mg) was calculated using the relationship $CL_{int} = kV/N$ where V is the incubation volume and N is the amount of protein per well. To measure CL_{int} in the presence of microsomal and cytosolic enzymes, the experiment was repeated using liver S9 fraction microsomes from male CD-1 mice sourced from Xenotech (Kansas City, KS), lot no. 1510255.

Hepatocyte Stability. Human cryopreserved hepatocytes were supplied by BioIVT (lot QZW, 10 pooled donors). Mouse cryopreserved hepatocytes were supplied by BioIVT (lot ZPG, pooled male CD-1). Vials of cryopreserved hepatocytes were removed from storage and thawed in a 37 °C water bath with gentle shaking, and then, the contents were poured into a 50 mL thawing medium conical tube. Vials were centrifuged at 100g for 10 min at room temperature. The thawing medium was aspirated, and hepatocytes were resuspended with a serum-free incubation medium to yield ~1.5 × 10^6 cells/mL. Cell viability and density were counted using AO/PI fluorescence staining, and then, cells were diluted with a serum-free incubation medium to a working cell density of 0.5 × 10^6 viable cells/mL. Aliquots of 198 μL of hepatocytes were dispensed into each well of a 96-well noncoated plate. The plate was placed in an incubator for approximately 10 min. Aliquots of 2 μL of the 100 μM test compound in duplicate and positive control were added into the respective wells of the noncoated 96-well plate to start the reaction. The final concentration of the test compound was 1 μM. The plate was placed in an incubator for the designed time points. Contents (25 μL) were transferred and mixed with six volumes (150 μL) of cold MeCN with IS (100 nM alprazolam, 200 nM labetalol, 200 nM caffeine, and 200 nM diclofenac) to terminate the reaction at time points of 0, 15, 30, 60, 90, and 120 min. Samples were centrifuged for 45 min at 3,220g, an aliquot of 100 μL of the supernatant was diluted with 100 μL of ultrapure H_2O, and the mixture was used for LC-MS/MS analysis. Peak areas were determined from extracted ion chromatograms, and the slope value, k, was determined by linear regression of the natural logarithm of the remaining percentage of the parent drug vs incubation time curve. The intrinsic clearance (CL_{int} in μL/min/10^6 cells) was calculated using the relationship $CL_{int} = kV/N$ where V is the incubation volume (0.2 mL) and N is the number of hepatocytes per well (0.1 × 10^6 cells). Scaling factors to convert CL_{int} from μL/min/10^6 cells to mL/min/kg were 2540 (human hepatocytes) and 11,800 (mouse hepatocytes).

Pharmacokinetics (PK). Male CD-1 mice (6−8 weeks, 20−30 g) were dosed by intravenous (i.v.) or interperitoneal (i.p.) administration. For i.v. administration, a single dose of the compound (1 mg/kg) was administered as a 5 mL/kg volume of a 0.2 mg/mL solution in NMP/solutol/PEG-400/normal saline ($v/v/v/v$, 10:5:30:55) to three mice. For i.p. administration, a single dose of the compound (10 mg/kg) was administered as a 10 mL/kg volume of a 1.0 mg/mL solution in 0.5% HPMC/0.2% Tween 80/99.3% H_2O or DMSO/PEG-400/saline ($v/v/v/v$, 10:30:60) to three mice. The mice had free access to water and food. Blood (0.03 mL) was collected from the dorsal metatarsal vein at 0.5, 1, 3, and 5 h time points (snapshot PK) or at 0.08, 0.25, 0.5, 1, 2, 4, 8, and 24 h (full PK). Blood from each sample was transferred into plastic microcentrifuge tubes containing EDTA-K2, mixed well, and then placed in a cold box prior to centrifugation. Blood samples were centrifuged at 4000g for 5 min at 4 °C to obtain plasma and then stored at −75 °C prior to analysis. Concentrations of the test compound in the plasma samples were determined using a Prominence LC-30AD, AB Sciex Triple Quan 5500 LC-MS/MS instrument fitted with a HALO 160A C18 column (2.7 μm, 2.1 × 50 mm) using a mobile phase of 5−95% MeCN in H_2O with 0.1% formic acid. PK parameters were calculated from the mean plasma concentration versus time by a noncompartmental model using WinNonlin 8.3 (Phoenix) to determine C_{max}, AUC_{last}, $t_{1/2}$, CL_{int}, and F.

For codosing studies, **2h** (10 mg/kg) was administered i.p. as a 10 mL/kg volume of a 1.0 mg/mL solution in DMSO/PEG-400/saline ($v/v/v/v$, 10:30:60). EA (10 or 30 mg/kg) was administered i.p. as a 1 mL/kg volume of a 30 mg/mL solution in NMP/PEG-400/water ($v/v/v$, 10:60:30) as a 6 h pretreatment and again at the time of dosing of **2h**. 1-ABT (100 mg/kg) was administered p.o. as a 10 mL/kg volume of a 10 mg/mL solution in saline as a 2 h pretreatment. Blood (0.03 mL) was collected from the dorsal metatarsal vein at 0.5, 1, 3, and 5 h time points and the level of **2h** in plasma determined by LC-MS/MS as described above. With this dosing protocol, no adverse clinical observations were recorded during the study.

General Synthetic Methods. All chemical reagents were commercially available except those whose synthesis is described below. All reaction mixtures and column eluents were monitored via analytical thin-layer chromatography (TLC) performed on precoated fluorescent silica gel plates, 200 μm with an F254 indicator; visualization was accomplished by UV light (254/365 nm). NMR spectra were obtained on a Bruker/AVANCE NEO 400 MHz instrument. LC-MS measurements were determined on Shimadzu LC-AB + LCMS-2020, Shimadzu LC-AD + LCMS-2020, Shimadzu

https://doi.org/10.1021/acsomega.3c05377
ACS Omega 2023, 8, 39546−39561

LC-AD xR + LCMS-2020, or Agilent 1200 + Infinitylab LC/MSD instruments. Purity was determined by HPLC measurement using a Shimadzu LC-20 + LCMS-2020 instrument fitted with an Agilent PoroShell 120 EC-C18 column (45 °C, 2.7 μm, 3.0 × 50 mm); 8 min chromatography ran 0.037% TFA in water/MeCN (19:1) (solvent A), 0.018% TFA/MeCN (solvent B), and gradient 0−60% (solvent B) over 6.0 min, held at 60% for 1.0 min, and returned to 0% (solvent B) for 1.0 min at a flow rate of 1.0 mL/min; 4 min chromatography ran 0.037% TFA in water/MeCN (19:1) (solvent A), 0.018% TFA/MeCN (solvent B), and gradient 10−80% (solvent B) over 3.0 min, held at 80% for 0.5 min, and returned to 0% (solvent B) for 0.5 min at a flow rate of 1.0 mL/min, which indicated that all final compounds were >95% pure.

General Procedure A. *Synthesis of Intermediate* ***y***. To a solution of *N*-(2-fluoro-5-nitrophenyl)propionamide (800 mg, 3.77 mmol) or *N*-(2-fluoro-5-nitrophenyl)acetamide (747 mg, 3.77 mmol) and an amine (3.77 mmol) in MeCN (8 mL) was added K_2CO_3 (1.56 g, 11.3 mmol) at 25 °C. The mixture was stirred at 100 °C for 10 h. The reaction mixture was concentrated in vacuo. Water (200 mL) was added, and the mixture was extracted with EtOAc (2× 250 mL). The combined organic phase was washed with brine (250 mL), dried over anhydrous Na_2SO_4, filtered, and concentrated in vacuo. To the resulting nitrobenzene (4.67 mmol) in MeOH (3 mL) was added 10% Pd/C (900 mg) under a N_2 atmosphere. The suspension was degassed, purged with H_2 three times, and then stirred under H_2 (15 psi) at 25 °C for 10 h. The reaction mixture was filtered through a celite pad. The pad was washed with MeOH (2× 8 mL), and the combined filtrate was concentrated in vacuo. The residue was purified by flash silica gel chromatography (eluent of 0−8%, MeOH/CH_2Cl_2) to yield intermediate **y**.

*(R)-N-(5-((3-Cyano-7-(cyclopropylamino)pyrazolo[1,5-a]-pyrimidin-5-yl)amino)-2-(3-(methylamino)piperidin-1-yl)-phenyl)propionamide (**1h**).* Intermediate **y** was synthesized from *tert*-butyl (*R*)-methyl(piperidin-3-yl)carbamate and *N*-(2-fluoro-5-nitrophenyl)propionamide by procedure A. To a solution of 5-chloro-7-(cyclopropylamino)pyrazolo[1,5-*a*]-pyrimidine-3-carbonitrile[5] (100 mg, 0.43 mmol) and intermediate **y** (170 mg, 0.43 mmol) in dioxane (3 mL) was added Cs_2CO_3 (418 mg, 1.28 mmol), BINAP (40 mg, 0.06 mmol), and $Pd(OAc)_2$ (14.0 mg, 0.06 mmol) at 25 °C. The mixture was degassed, purged with N_2, and then heated in a microwave reactor at 130 °C for 0.5 h. The reaction mixture was concentrated in vacuo, and the residue was purified by flash silica gel chromatography (eluent of 0−4%, MeOH/CH_2Cl_2). To the product in CH_2Cl_2 (5 mL) was added TFA (7 mL), and the mixture was stirred at 25 °C for 2 h. The reaction mixture was concentrated in vacuo, and the residue was purified by prep-HPLC (column: Xtimate C18 150 × 40 mm × 10 μm; mobile phase: [water (HCO_2H)-MeCN]; B%: 15−45%, 10 min). Compound **1h** (66.3 mg, 11.3%) was obtained as a white solid. ^{1}H NMR (400 MHz, DMSO-d_6) δ 9.65 (s, 1H), 9.33 (br s, 1H), 8.44 (s, 1H), 8.33 (s, 1H), 8.19 (s, 1H), 8.04 (d, J = 2.4 Hz, 1H), 7.82 (d, J = 7.2 Hz, 1H), 7.09 (d, J = 8.4 Hz, 1H), 6.03 (s, 1H), 3.13 (br s, 1H), 3.05 (d, J = 10.4 Hz, 1H), 2.89−2.80 (m, 2H), 2.60−2.58 (m, 2H), 2.52−2.51 (m, 1H), 2.48−2.44 (m, 4H), 1.92−1.91 (m, 1H), 1.75 (s, 2H), 1.62−1.60 (m, 1H), 1.12 (t, J = 7.6 Hz, 3H), 0.80−0.79 (m, 2H), 0.72−0.70 (m, 2H). ^{13}C NMR (101 MHz, DMSO-d_6) δ 172.04, 165.85, 156.77, 150.78, 148.07, 144.88, 137.77, 136.07, 132.78, 119.97, 114.74, 76.13, 54.06, 52.95, 38.69, 30.66, 29.41, 23.17, 9.79, 6.39. HPLC R_t = 3.656 min in 8 min chromatography, purity 99.6%. LC-MS R_t = 1.925 min in 4 min chromatography, purity 98.0%, MS ESI calcd. for 473.27 $[M + H]^+$ 474.27, found 474.4.

*(S)-N-(5-((3-Cyano-7-(cyclopropylamino)pyrazolo[1,5-a]-pyrimidin-5-yl)amino)-2-(3-(methylamino)piperidin-1-yl)-phenyl)propionamide (**1i**).* Intermediate **y** was synthesized from *tert*-butyl (*S*)-methyl(piperidin-3-yl)carbamate and *N*-(2-fluoro-5-nitrophenyl)propionamide by procedure A. To a solution of 5-chloro-7-(cyclopropylamino)pyrazolo[1,5-*a*]-pyrimidine-3-carbonitrile[5] (112 mg, 0.48 mmol) and intermediate **y** (200 mg, 0.53 mmol) in dioxane (3 mL) was added Cs_2CO_3 (502 mg, 1.53 mmol), BINAP (48 mg, 0.07 mmol), and $Pd(OAc)_2$ (16.8 mg, 0.07 mmol) at 25 °C. The mixture was degassed, purged with N_2, and heated in a microwave reactor at 130 °C for 0.5 h. The reaction mixture was concentrated in vacuo, and the residue was purified by flash silica gel chromatography (eluent of 0−4%, MeOH/CH_2Cl_2). To the product in CH_2Cl_2 (5 mL) was added TFA (7 mL), and the mixture was stirred at 25 °C for 2 h. The reaction mixture was concentrated in vacuo, and the residue was purified by prep-HPLC (column: Xtimate C18 150 × 40 mm × 10 μm; mobile phase: [water (HCO_2H)-MeCN]; B%: 0−38%, 36 min). Compound **1i** (115 mg, 37.0%) was obtained as a yellow solid. ^{1}H NMR (400 MHz, DMSO-d_6) δ 9.65 (s, 1H), 9.09 (s, 1H), 8.43−8.36 (m, 1H), 8.34 (s, 1H), 8.20 (s, 1H), 8.07−8.01 (m, 1H), 7.89−7.78 (m, 1H), 7.12 (d, J = 8.8 Hz, 1H), 6.03 (s, 1H), 3.24 (s, 1H), 3.12−3.05 (m, 1H), 2.93−2.84 (m, 1H), 2.83−2.75 (m, 1H), 2.68−2.54 (m, 5H), 2.48−2.41 (m, 2H), 1.95−1.60 (m, 4H), 1.13 (t, J = 7.6 Hz, 3H), 0.84−0.66 (m, 4H). ^{13}C NMR (101 MHz, DMSO-d_6) δ: 172.16, 165.58, 156.97, 150.97, 148.26, 145.06, 137.96, 136.25, 132.97, 120.21, 115.33, 114.91, 76.32, 54.47, 53.83, 53.02, 31.24, 29.65, 23.36, 21.77, 9.95, 6.57. HPLC R_t = 3.612 min in 8 min chromatography, purity 99.6%. LC-MS R_t = 1.567 min in 4 min chromatography, purity 100.0%, MS ESI calcd. for 473.3 $[M + H]^+$ 474.3, found 474.5.

*(R)-N-(5-((3-Cyano-7-(cyclopropylamino)pyrazolo[1,5-a]-pyrimidin-5-yl)amino)-2-(3-(methylamino)piperidin-1-yl)-phenyl)acetamide (**2b**).* Intermediate **y** was synthesized from *tert*-butyl (*R*)-methyl(piperidin-3-yl)carbamate and *N*-(2-fluoro-5-nitrophenyl)acetamide by procedure A. To a solution of 5-chloro-7-(cyclopropylamino)pyrazolo[1,5-*a*]pyrimidine-3-carbonitrile[5] (112 mg, 0.48 mmol) and intermediate **y** (200 mg, 0.55 mmol) in dioxane (3 mL) was added Cs_2CO_3 (541 mg, 1.65 mmol), BINAP (51 mg, 0.08 mmol), and $Pd(OAc)_2$ (17.9 mg, 0.08 mmol) at 25 °C. The mixture was degassed, purged with N_2, and heated in a microwave reactor at 130 °C for 0.5 h. The reaction mixture was concentrated in vacuo, and the residue was purified by flash silica gel chromatography (eluent of 0−32%, EtOAc/petroleum ether) to give the product. To the product in CH_2Cl_2 (5 mL) was added TFA (7 mL), and the mixture was stirred at 25 °C for 2 h. The reaction mixture was concentrated in vacuo, and the residue was purified by prep-HPLC (column: Phenomenex C18 75 × 30 mm × 3 μm; mobile phase: [water (HCO_2H)-MeCN]; B%: 2−32%, 24 min). Compound **2b** (32.8 mg, 27.4%) was obtained as a white solid. ^{1}H NMR (400 MHz, DMSO-d_6) δ 9.63 (s, 1H), 9.41 (s, 1H), 8.41 (s, 1H), 8.32 (s, 1H), 8.16 (s, 1H), 7.99 (d, J = 1.6 Hz, 1H), 7.83 (d, J = 6.4 Hz, 1H), 7.10 (d, J = 8.8 Hz, 1H), 6.03 (s, 1H), 3.22 (s, 1H), 3.06 (d, J = 11.2 Hz, 1H), 2.93 (d, J = 8.4 Hz, 1H), 2.84 (d, J = 11.2 Hz, 1H), 2.58 (s, 2H), 2.53 (s, 3H), 2.18 (s, 3H), 1.95 (s, 1H),

https://doi.org/10.1021/acsomega.3c05377
ACS Omega 2023, 8, 39546−39561

1.79 (s, 2H), 1.67−1.56 (m, 1H), 0.80 (d, J = 6.8 Hz, 2H), 0.70 (d, J = 2.8 Hz, 2H). ^{13}C NMR (101 MHz, DMSO-d_6) δ: 168.62, 163.65, 156.97, 150.98, 148.26, 145.08, 137.91, 136.26, 133.03, 120.20, 115.42, 114.96, 76.32, 54.08, 53.19, 40.15, 39.99, 39.78, 24.09, 23.36, 6.59. HPLC R_t = 3.321 min in 8 min chromatography, purity 99.9%. LC-MS R_t = 1.551 min in 4 min chromatography, purity 99.8%, MS ESI calcd. for 459.25 $[M + H]^+$ 460.25, found 460.4.

*(S)-N-(5-((3-Cyano-7-(cyclopropylamino)pyrazolo[1,5-a]-pyrimidin-5-yl)amino)-2-(3-(methylamino)piperidin-1-yl)-phenyl)acetamide (**2c**).* Intermediate **y** was synthesized from *tert*-butyl (*S*)-methyl(piperidin-3-yl)carbamate and *N*-(2-fluoro-5-nitrophenyl)acetamide by procedure A. To a solution of 5-chloro-7-(cyclopropylamino)pyrazolo[1,5-*a*]pyrimidine-3-carbonitrile[5] (237 mg, 1.02 mmol) and intermediate **y** (460 mg, 1.27 mmol) in dioxane (6 mL) was added Cs_2CO_3 (1.0 g, 1.65 mmol), BINAP (94.8 mg, 0.14 mmol), and $Pd(OAc)_2$ (33.2 mg, 0.14 mmol) at 25 °C. The mixture was degassed, purged with N_2, and heated in a microwave reactor at 130 °C for 0.5 h. The reaction mixture was concentrated in vacuo, and the residue was purified by flash silica gel chromatography (eluent of 0−3%, MeOH/CH_2Cl_2). To the product in CH_2Cl_2 (5 mL) was added TFA (7 mL), and the mixture was stirred at 25 °C for 2 h. The reaction mixture was concentrated in vacuo, and the residue was purified by prep-HPLC (column: Xtimate C18 100 × 30 mm × 10 μm; mobile phase: [water (HCO_2H)-MeCN]; B%: 30−50%, 10 min). Compound **2c** (58 mg, 27.4%) was obtained as a white solid. ^{1}H NMR (400 MHz, DMSO-d_6) δ 9.64 (s, 1H), 9.38−9.21 (m, 1H), 8.39−8.30 (m, 1H), 8.17 (s, 1H), 7.97 (s, 1H), 7.89−7.77 (m, 1H), 7.10 (d, J = 8.8 Hz, 1H), 6.03 (s, 1H), 3.11−3.03 (m, 2H), 3.02−2.90 (m, 2H), 2.89−2.82 (m, 1H), 2.62−2.53 (m, 5H), 2.20 (s, 3H), 2.06−1.94 (m, 1H), 1.89−1.72 (m, 2H), 1.67−1.58 (m, 1H), 0.84−0.76 (m, 2H), 0.73−0.66 (m, 2H). ^{13}C NMR (101 MHz, DMSO-d_6) δ: 168.66, 162.94, 156.95, 150.96, 148.25, 145.07, 137.91, 136.26, 132.85, 120.17, 115.48, 114.94, 113.94, 76.32, 54.13, 53.14, 39.99, 30.59, 24.20, 23.36, 6.58. HPLC R_t = 3.324 min in 8 min chromatography, purity 99.2%. LC-MS R_t = 1.549 min in 4 min chromatography, purity 99.6%, MS ESI calcd. for 459.25 $[M + H]^+$ 460.25, found 460.4.

*(R)-N-(5-((3-Cyano-7-(cyclopropylamino)pyrazolo[1,5-a]-pyrimidin-5-yl)amino)-2-(3-(methylamino)pyrrolidin-1-yl)-phenyl)acetamide (**2d**).* Intermediate **y** was synthesized from *tert*-butyl (*R*)-methyl(pyrrolidin-3-yl)carbamate and *N*-(2-fluoro-5-nitrophenyl)acetamide by procedure A. To a solution of 5-chloro-7-(cyclopropylamino)pyrazolo[1,5-*a*]pyrimidine-3-carbonitrile[5] (134 mg, 0.57 mmol) and intermediate **y** (250 mg, 0.72 mmol) in dioxane (3 mL) was added Cs_2CO_3 (0.5 g, 0.82 mmol), BINAP (47.4 mg, 0.07 mmol), and $Pd(OAc)_2$ (16.6 mg, 0.07 mmol) at 25 °C. The mixture was degassed, purged with N_2, and heated in a microwave reactor at 130 °C for 0.5 h. The reaction mixture was concentrated in vacuo, and the residue was purified by prep-HPLC (column: Waters Torus 2-PIC 150 mm × 19 mm × 5 μm; mobile phase: [Heptane-EtOH (0.1% NH_3/H_2O)]; B%: 10−50%, 5 min) to give the product as a yellow solid. To the product in CH_2Cl_2 (5 mL) was added TFA (7 mL), and the mixture was stirred at 25 °C for 2 h. The reaction mixture was concentrated in vacuo, and the residue was purified by prep-HPLC (column: Xtimate C18 100 mm × 30 mm × 10 μm; mobile phase: [water (HCO_2H)-MeCN]; B%: 25−45%, 10 min). Compound **2d** (20 mg, 30.2%) was obtained as a white solid. ^{1}H NMR (400 MHz, MeOD-d_4) δ 9.56 (s, 1H), 9.30 (s, 1H), 8.46−8.28 (m, 2H), 8.16 (s, 1H), 7.93−7.60 (m, 2H), 7.02 (d, J = 8.4 Hz, 1H), 5.99 (s, 1H), 3.55−3.50 (m, 1H), 3.34−3.09 (m, 4H), 2.95−2.84 (m, 1H), 2.61−2.51 (m, 4H), 2.26−2.06 (m, 4H), 1.9−1.86 (m, 1H), 0.86−0.76 (m, 2H), 0.75−0.66 (m, 2H). ^{13}C NMR (101 MHz, DMSO-d_6) δ: 168.49, 157.01, 151.02, 148.19, 145.00, 134.54, 130.86, 118.11, 116.30, 114.95, 76.17, 57.99, 54.44, 49.20, 39.99, 23.89, 23.32, 6.55. HPLC R_t = 3.063 min in 8 min chromatography, purity 99.8%. LC-MS R_t = 1.422 min in 4 min chromatography, purity 99.9%, MS ESI calcd. for 445.23 $[M + H]^+$ 446.23, found 446.4.

*(S)-N-(5-((3-Cyano-7-(cyclopropylamino)pyrazolo[1,5-a]-pyrimidin-5-yl)amino)-2-(3-(methylamino)pyrrolidin-1-yl)-phenyl)acetamide (**2e**).* Intermediate **y** was synthesized from *tert*-butyl (*S*)-methyl(pyrrolidin-3-yl)carbamate and *N*-(2-fluoro-5-nitrophenyl)acetamide by procedure A. To a solution of 5-chloro-7-(cyclopropylamino)pyrazolo[1,5-*a*]pyrimidine-3-carbonitrile[5] (520 mg, 2.23 mmol) and intermediate **y** (930 mg, 2.67 mmol) in dioxane (15 mL) was added Cs_2CO_3 (2.2 g, 6.7 mmol), BINAP (207 mg, 0.31 mmol), and $Pd(OAc)_2$ (72.7 mg, 0.31 mmol) at 25 °C. The mixture was degassed, purged with N_2, and heated in a microwave reactor at 130 °C for 0.5 h. The reaction mixture was concentrated in vacuo, and the residue was purified by flash silica gel chromatography (eluent of 0−51%, EtOAc/petroleum ether) to give the product as a gray solid. To the product in CH_2Cl_2 (5 mL) was added TFA (7 mL), and the mixture was stirred at 25 °C for 2 h. The reaction mixture was concentrated in vacuo, and the residue was purified by prep-HPLC (column: Welch Xtimate C18 150 × 30 mm × 5 μm; mobile phase: [water (HCO_2H)-MeCN]; B %: 0−90%, 14 min). Compound **2e** (30.6 mg, 16.2%) was obtained as a light-yellow solid. ^{1}H NMR (400 MHz, DMSO-d_6) δ 9.59 (s, 1H), 9.42 (s, 1H), 8.41 (s, 1H), 8.33 (s, 1H), 8.18 (s, 1H), 7.86 (s, 1H), 7.76 (s, 1H), 7.03 (d, J = 8.8 Hz, 1H), 6.00 (s, 1H), 3.56 (s, 1H), 3.30 (d, J = 4.4 Hz, 1H), 3.21−3.16 (m, 1H), 3.16−3.11 (m, 1H), 2.82 (q, J = 8.0 Hz, 1H), 2.57 (s, 1H), 2.52−2.51 (m, 3H), 2.26−2.17 (m, 1H), 2.14 (s, 3H), 1.97 (s, 1H), 0.84−0.76 (m, 2H), 0.72−0.66 (m, 2H). ^{13}C NMR (101 MHz, DMSO-d_6) δ 168.51, 165.64, 157.00, 151.01, 148.19, 145.00, 134.62, 131.13, 118.19, 116.20, 115.48, 114.95, 76.16, 76.04, 57.88, 54.30, 49.20, 31.64, 28.59, 23.90, 23.32, 6.55. HPLC R_t = 3.080 min in 8 min chromatography, purity 99.4%. LC-MS R_t = 1.420 min in 4 min chromatography, purity 99.7%, MS ESI calcd. for 445.23 $[M + H]^+$ 446.23, found 446.4.

*(S)-N-(5-((3-Cyano-7-(cyclopropylamino)pyrazolo[1,5-a]-pyrimidin-5-yl)amino)-2-(methyl(pyrrolidin-2-ylmethyl)-amino)phenyl)acetamide (**2f**).* Intermediate **y** was synthesized from *tert*-butyl (*S*)-2-((methylamino)methyl)pyrrolidine-1-carboxylate and *N*-(2-fluoro-5-nitrophenyl)acetamide by procedure A. To a solution of 5-chloro-7-(cyclopropylamino)-pyrazolo[1,5-*a*]pyrimidine-3-carbonitrile[5] (52.0 mg, 0.220 mmol) and intermediate **y** (100 mg, 0.280 mmol) in dioxane (2 mL) was added Cs_2CO_3 (209 mg, 0.64 mmol), BINAP (20 mg, 0.03 mmol), and $Pd(OAc)_2$ (7.0 mg, 0.03 mmol) at 25 °C. The mixture was degassed, purged with N_2, and heated in a microwave reactor at 130 °C for 0.5 h. The reaction mixture was concentrated in vacuo, and the residue was purified by flash silica gel chromatography (eluent of 0−2%, MeOH/CH_2Cl_2) to give the product as a brown solid. To the product in CH_2Cl_2 (5 mL) was added TFA (7 mL), and the mixture was stirred at 25 °C for 2 h. The reaction mixture was concentrated in vacuo, and the residue was purified by prep-HPLC (column: Xtimate C18 150 mm × 40 mm × 10 μm;

https://doi.org/10.1021/acsomega.3c05377
ACS Omega 2023, 8, 39546−39561

mobile phase: [water (NH_4HCO_3)-MeCN]; B%: 22−62%, 25 min). Compound **2f** (25.0 mg, 30.3%) was obtained as a yellow solid. ^{1}H NMR (400 MHz, DMSO-d_6) δ 10.76−10.36 (m, 1H), 9.61 (s, 1H), 8.37−8.30 (m, 2H), 8.16 (s, 1H), 7.89−7.77 (m, 1H), 7.17 (d, J = 8.8 Hz, 1H), 6.05 (s, 1H), 3.48−3.39 (m, 1H), 3.36−3.33 (m, 2H), 3.01−2.91 (m, 1H), 2.85−2.74 (m, 1H), 2.66 (s, 3H), 2.61−2.54 (m, 1H), 2.14 (s, 3H), 1.92−1.58 (m, 3H), 1.30−1.17 (m, 1H), 0.83−0.75 (m, 2H), 0.74−0.67 (m, 2H). ^{13}C NMR (101 MHz, DMSO-d_6) δ: 168.17, 156.98, 150.95, 148.20, 145.02, 137.56, 135.98, 132.98, 120.22, 114.90, 76.25, 65.21, 59.77, 51.82, 31.69, 24.21, 23.32, 22.38, 6.55. HPLC R_t= 3.426 min in 8 min chromatography, purity 99.4%. LC-MS R_t= 2.058 min in 4 min chromatography, purity 95.5%, MS ESI calcd. for 445.23 $[M + H]^+$ 446.23, found 460.3.

*N-(5-((3-Cyano-7-(cyclopropylamino)pyrazolo[1,5-a]-pyrimidin-5-yl)amino)-2-(piperazin-1-yl)phenyl)acetamide (**2g**).* Intermediate **y** was synthesized from *tert*-butyl piperazine-1-carboxylate and *N*-(2-fluoro-5-nitrophenyl)acetamide by procedure A. To a solution of 5-chloro-7-(cyclopropylamino)pyrazolo[1,5-*a*]pyrimidine-3-carbonitrile[5] (302 mg, 1.29 mmol) and intermediate **y** (433 mg, 1.29 mmol) in dioxane (9 mL) was added Cs_2CO_3 (1.25 g, 3.84 mmol), BINAP (120 mg, 0.18 mmol), and $Pd(OAc)_2$ (42.0 mg, 0.18 mmol) at 25 °C. The mixture was degassed, purged with N_2, and heated in a microwave reactor at 130 °C for 0.5 h. The reaction mixture was concentrated in vacuo, and the residue was purified by flash silica gel chromatography (eluent of 30−70%, EtOAc/petroleum ether) to give the product as a brown solid. To the product in CH_2Cl_2 (5 mL) was added TFA (7 mL), and the mixture was stirred at 25 °C for 2 h. The reaction mixture was concentrated in vacuo, and the residue was purified by prep-HPLC (column: Xtimate C18 100 mm × 30 mm × 10 μm; mobile phase: [water (HCO_2H)-MeCN]; B%: 5−96%, 10 min; B%: 4−34%, 10 min). Compound **2g** (178.4 mg, 27.4%) was obtained as a light-yellow solid. ^{1}H NMR (400 MHz, DMSO-d_6) δ 9.68 (s, 1H), 8.92 (s, 1H), 8.33 (m, 1H), 8.48−8.31 (m, 1H), 8.12−7.99 (m, 1H), 7.89 (d, J = 6.8 Hz, 1H), 7.15 (d, J = 9.2 Hz, 1H), 6.03 (s, 1H), 3.35−3.22 (m, 4H), 3.02−2.88 (m, 4H), 2.63−2.55 (m, 1H), 2.16 (s, 3H), 0.87−0.76 (m, 2H), 0.73−0.66 (m, 2H). ^{13}C NMR (101 MHz, DMSO-d_6) δ: 168.53, 156.91, 150.90, 148.24, 145.06, 136.92, 136.49, 133.12, 120.45, 115.14, 114.90, 112.84, 76.38, 49.29, 43.46, 39.99, 24.25, 23.34, 6.56. HPLC R_t= 1.599 min in 6 min chromatography, purity 95.6%. LC-MS R_t= 1.003 min in 4 min chromatography, purity 95.9%, MS ESI calcd. for 431.22 $[M + H]^+$ 432.22, found 432.2.

*(S)-N-(5-((3-Cyano-7-(cyclopropylamino)pyrazolo[1,5-a]-pyrimidin-5-yl)amino)-2-(3-hydroxypiperidin-1-yl)phenyl)-acetamide (**2i**).* Intermediate **y** was synthesized from (*S*)-piperidin-3-ol hydrochloride and *N*-(2-fluoro-5-nitrophenyl)-acetamide by procedure A. To a solution of 5-chloro-7-(cyclopropylamino)pyrazolo[1,5-*a*]pyrimidine-3-carbonitrile[5] (75 mg, 0.32 mmol) and intermediate **y** (100 mg, 0.40 mmol) in dioxane (3 mL) was added Cs_2CO_3 (388 mg, 1.19 mmol), BINAP (37.2 mg, 0.05 mmol), and $Pd(OAc)_2$ (12.7 mg, 0.05 mmol) at 25 °C. The mixture was degassed, purged with N_2, and heated in a microwave reactor at 130 °C for 0.5 h. The reaction mixture was concentrated in vacuo, and the residue was purified by prep-HPLC (column: Xtimate C18 150 × 30 mm × 5 μm; mobile phase: [water (NH_4HCO_3)-MeCN]; B%: 20−60%, 25 min) to give compound **2i** (25.0 mg, 13.8%) as a white solid. ^{1}H NMR (400 MHz, DMSO-d_6) δ 9.61 (s, 1H), 9.04 (s, 1H), 8.33 (s, 1H), 8.19−8.04 (m, 2H), 7.88−7.83 (m, 1H), 7.08 (d, J = 8.4 Hz, 1H), 6.03 (s, 1H), 5.09−4.87 (m, 1H), 3.80 (s, 1H), 2.86−2.76 (m, 2H), 2.75−2.67 (m, 1H), 2.65−2.54 (m, 2H), 2.13 (s, 3H), 1.95−1.81 (m, 1H), 1.77−1.55 (m, 2H), 1.54−1.42 (m, 1H), 0.83−0.75 (m, 2H), 0.74−0.67 (m, 2H). ^{13}C NMR (101 MHz, DMSO-d_6) δ: 168.74, 157.10, 151.04, 148.24, 145.08, 137.49, 136.04, 134.09, 120.57, 115.02, 114.57, 111.52, 76.29, 48.67, 45.67, 28.83, 24.17, 23.38, 6.61. HPLC R_t= 3.771 min in 8 min chromatography, purity 99.0%. LC-MS R_t= 2.050 min in 4 min chromatography, purity 98.3%, MS ESI calcd. for 446.22 $[M + H]^+$ 447.22, found 447.3.

*N-(5-((3-Cyano-7-(cyclopropylamino)pyrazolo[1,5-a]-pyrimidin-5-yl)amino)-2-(methyl(oxetan-3-yl)amino)-phenyl)acetamide (**2j**).* Intermediate **y** was synthesized from *N*-methyloxetan-3-amine and *N*-(2-fluoro-5-nitrophenyl)-acetamide by procedure A. To a solution of 5-chloro-7-(cyclopropylamino)pyrazolo[1,5-*a*]pyrimidine-3-carbonitrile[5] (96.0 mg, 0.410 mmol) and intermediate **y** (120 mg, 0.510 mmol) in dioxane (3 mL) was added Cs_2CO_3 (398 mg, 1.21 mmol), BINAP (38.1 mg, 0.06 mmol), and $Pd(OAc)_2$ (13.3 mg, 0.06 mmol) at 25 °C. The mixture was degassed, purged with N_2, and heated in a microwave reactor at 130 °C for 0.5 h. The reaction mixture was concentrated in vacuo, and the residue was purified by prep-HPLC (column: Xtimate C18 150 × 40 mm × 10 μm; mobile phase: [water (NH_4HCO_3)-MeCN]; B%: 18−58%, 25 min). Compound **2j** (4.70 mg, 5.88%) was obtained as a yellow solid. ^{1}H NMR (400 MHz, DMSO-d_6) δ 9.65 (s, 1H), 9.06 (s, 1H), 8.34 (s, 1H), 8.19 (s, 1H), 8.10 (s, 1H), 7.86 (d, J = 8.0 Hz, 1H), 6.97 (d, J = 8.8 Hz, 1H), 6.03 (s, 1H), 4.64−4.56 (m, 2H), 4.44−4.37 (m, 2H), 4.38−4.30 (m, 1H), 2.62−2.54 (m, 1H), 2.46 (s, 3H), 2.18 (s, 3H), 0.85−0.76 (m, 2H), 0.75−0.67 (m, 2H). HPLC R_t = 4.106 min in 8 min chromatography, purity 99.9%. LC-MS R_t = 2.487 min in 4 min chromatography, purity 97.9%, MS ESI calcd. for 432.2, $[M + H]^+$ 433.2, found 433.2.

*(S)-N-(5-((3-Cyano-7-(cyclopropylamino)pyrazolo[1,5-a]-pyrimidin-5-yl)amino)-2-(methyl(tetrahydrofuran-3-yl)-amino)phenyl)acetamide (**2k**).* Intermediate **y** was synthesized from (*S*)-*N*-methyltetrahydrofuran-3-amine hydrochloride and *N*-(2-fluoro-5-nitrophenyl)acetamide by procedure A. To a solution of 5-chloro-7-(cyclopropylamino)pyrazolo[1,5-*a*]pyrimidine-3-carbonitrile[5] (84.3 mg, 0.361 mmol) and intermediate **y** (90.0 mg, 0.361 mmol) in dioxane (2 mL) was added Cs_2CO_3 (470 mg, 1.44 mmol), BINAP (33.7 mg, 0.054 mmol), and $Pd(OAc)_2$ (12.2 mg, 0.054 mmol) 25 °C. The mixture was degassed, purged with N_2 three times, and then heated in a microwave reactor at 120 °C for 2 h. The mixture was filtered and concentrated to give a residue that was purified by prep-HPLC purification (column: Phenomenex luna C18 150 × 25 mm × 10 μm; mobile phase: [water (HCO_2H)-MeCN]; B%: 30−60%, 10 min) to give product **2k** (19.3 mg, 11.6% yield) as a white solid. ^{1}H NMR (400 MHz, DMSO-d_6) δ 9.68 (s, 1H), 9.06 (s, 1H), 8.35 (s, 1H), 8.24−8.15 (m, 2H), 7.99−7.88 (m, 1H), 7.30 (d, J = 8.8 Hz, 1H), 6.06 (s, 1H), 3.89−3.75 (m, 1H), 3.71−3.62 (m, 3H), 3.57−3.48 (m, 1H), 2.60−2.52 (m, 1H), 2.53 (s, 3H), 2.14 (s, 3H), 2.00−1.88 (m, 1H), 1.86−1.74 (m, 1H), 0.86−0.78 (m, 2H), 0.76−0.68 (m, 2H). ^{13}C NMR (101 MHz, DMSO-d_6) δ: 171.96, 155.87, 149.91, 149.11, 145.60, 139.08, 138.85, 129.13, 119.45, 117.37, 114.13, 78.81, 77.86, 39.99, 39.00, 23.50, 6.58. LC-MS: R_t= 0.393 min in 0.8 min chromatography, purity 100.0%, MS ESI calcd. for $C_{23}H_{27}N_8O_2$ $[M + H]^+$ 447.22,

https://doi.org/10.1021/acsomega.3c05377
ACS Omega 2023, 8, 39546−39561

found 447.1. HPLC: R_t= 1.850 min in 4 min chromatography, purity 97.4%.

*(R)-N-(5-((3-Cyano-7-(cyclopropylamino)pyrazolo[1,5-a]-pyrimidin-5-yl)amino)-2-(methyl(tetrahydrofuran-3-yl)-amino)phenyl)acetamide (**2l**).* Intermediate **y** was synthesized from (*R*)-*N*-methyltetrahydrofuran-3-amine hydrochloride and *N*-(2-fluoro-5-nitrophenyl)acetamide by procedure A. To a solution of 5-chloro-7-(cyclopropylamino)pyrazolo[1,5-*a*]-pyrimidine-3-carbonitrile[5] (98 mg, 0.421 mmol) and intermediate **y** (105 mg, 0.421 mmol) in dioxane (5 mL) was added Cs_2CO_3 (411 mg, 1.26 mmol), BINAP (39.3 mg, 0.063 mmol), and $Pd(OAc)_2$ (14.2 mg, 0.063 mmol) 25 °C. The mixture was degassed, purged with N_2 three times, and then heated in a microwave reactor at 120 °C for 2 h. The reaction mixture was filtered and concentrated under reduced pressure to give a residue that was purified by prep-TLC (SiO_2, CH_2Cl_2/MeOH = 20/1), and the crude product was purified by prep-HPLC (column: Phenomenex Luna C18 150 × 25 mm × 10 μm; mobile phase: [water (HCO_2H)-MeCN]; B%: 29−59%, 8 min). Compound **2l** (18.2 mg, 9.71% yield) was obtained as a white solid. ^{1}H NMR (400 MHz, DMSO-d_6) δ 9.67 (s, 1H), 8.98 (s, 1H), 8.34 (s, 1H), 8.17 (d, J = 12.8 Hz, 2H), 7.92 (br d, J = 5.2 Hz, 1H), 7.29 (d, J = 8.8 Hz, 1H), 6.05 (s, 1H), 3.88−3.79 (m, 1H), 3.71−3.62 (m, 3H), 3.56−3.47 (m, 1H), 2.62−2.53 (m, 1H), 2.52 (s, 3H), 2.14 (s, 3H), 1.99−1.86 (m, 1H), 1.84−1.76 (m, 1H), 0.83−0.77 (m, 2H), 0.73−0.68 (m, 2H). ^{13}C NMR (101 MHz, DMSO-d_6) δ: 172.48, 156.90, 150.87, 148.20, 145.05, 138.50, 137.18, 134.98, 123.04, 114.87, 76.44, 70.96, 67.04, 63.59, 41.65, 30.73, 23.31, 6.53. LC-MS R_t = 0.395 min in 0.8 min chromatography, purity 44.5%, MS ESI calcd. for 446.50 $[M + H]^+$ 447.50, found 447.1. HPLC: R_t = 1.011 min in 4 min chromatography, purity 96.7%.

*(R)-N-(5-((3-Cyano-7-(cyclopropylamino)pyrazolo[1,5-a]-pyrimidin-5-yl)amino)-2-((tetrahydro-2H-pyran-3-yl)-amino)phenyl)acetamide (**2m**).* Intermediate **y** was synthesized from (*R*)-tetrahydro-2H-pyran-3-amine hydrochloride and *N*-(2-fluoro-5-nitrophenyl)acetamide by procedure A. To a solution of 5-chloro-7-(cyclopropylamino)pyrazolo[1,5-*a*]-pyrimidine-3-carbonitrile[5] (220 mg, 0.943 mmol) and intermediate **y** (235 mg, 0.943 mmol) in dioxane (6 mL) was added Cs_2CO_3 (915 mg, 2,83 mmol), BINAP (87.6 mg, 0.13 mmol), and $Pd(OAc)_2$ (30.2 mg, 0.13 mmol) 25 °C. The mixture was degassed, purged with N_2 three times, and then heated in a microwave reactor at 120 °C for 2 h. The mixture was filtered and concentrated to give a residue that was purified by prep-HPLC purification (column: Phenomenex Luna C18 150 mm × 25 mm × 10 μm; mobile phase: [water (HCO_2H)-MeCN]; B%: 26−56%, 10 min, and column: Phenomenex C18 150 × 25 mm × 10 μm; mobile phase: [water (NH_4HCO_3)-MeCN]; B%: 22−52%, 14 min) to give compound **2m** (10 mg, 22.40 μmol, 2.38% yield) as an off-white solid. ^{1}H NMR (400 MHz, DMSO-d_6) δ 9.33 (s, 1H), 9.19 (s, 1H), 8.29 (s, 1H), 8.09 (s, 1H), 7.45 (s, 1H), 7.39 (s, 1H), 6.73 (d, J = 8.8 Hz, 1H), 5.90 (s, 1H), 4.54 (d, J = 8.0 Hz, 1H), 3.89−3.82 (m, 1H), 3.75−3.67 (m, 1H), 3.42−3.38 (m, 2H), 3.27−3.11 (m, 1H), 2.59−2.52 (m, 1H), 2.06 (s, 3H), 2.01−1.93 (m, 1H), 1.75−1.67 (m, 1H), 1.63−1.45 (m, 2H), 0.82−0.74 (m, 2H), 0.72−0.65 (m, 2H). HPLC: R_t = 1.670 min in 4 min chromatography, purity 97.6%. LC-MS R_t = 0.365 min in 0.8 min chromatography, purity 99.1%, MS ESI calcd. for 446.22 $[M + H]^+$ 447.22, we found 447.2.

*N-(5-((3-Cyano-7-(cyclopropylamino)pyrazolo[1,5-a]-pyrimidin-5-yl)amino)-2-(methyl(oxetan-3-ylmethyl)-amino)phenyl)acetamide (**2n**).* Intermediate **y** was synthesized from *N*-methyl-1-(oxetan-3-yl)methanamine hydrochloride and *N*-(2-fluoro-5-nitrophenyl)acetamide by procedure A. To a solution of 5-chloro-7-(cyclopropylamino)pyrazolo[1,5-*a*]pyrimidine-3-carbonitrile[5] (293 mg, 1.26 mmol) and intermediate **y** (313 mg, 1.26 mmol) in dioxane (10 mL) was added Cs_2CO_3 (1.64 g, 5.02 mmol), BINAP (117 mg, 0.188 mmol), and $Pd(OAc)_2$ (42.2 mg, 0.188 mmol) at 25 °C. The mixture was degassed, purged with N_2, and then heated in a microwave reactor at 120 °C for 2 h. The reaction mixture was diluted with CH_2Cl_2/MeOH (10/1, 30 mL) and then filtered, and the filtrate was concentrated to give a crude product that was purified by flash silica gel chromatography (eluent of 30−80% EtOAc/petroleum ether). The crude product was further purified by prep-HPLC (column: Phenomenex Luna C18 150 × 25 mm × 10 μm; mobile phase: [water (HCO_2H)-MeCN]; B%: 22−52%, 10 min) to give compound **2n** (150.6 mg, 32.9%) as a light-yellow solid. ^{1}H NMR (400 MHz, DMSO-d_6) δ 9.56 (s, 1H), 8.93 (s, 1H), 8.33 (s, 1H), 8.17 (s, 1H), 8.10 (s, 1H), 7.88 (d, J = 7.2 Hz, 1H), 7.24 (d, J = 8.8 Hz, 1H), 6.04 (s, 1H), 4.53 (t, J = 7.2 Hz, 2H), 4.22 (t, J = 6.0 Hz, 2H), 3.15−3.09 (m, 2H), 3.08−3.01 (m, 1H), 2.56 (s, 3H), 2.55−2.51 (m, 1H), 2.12 (s, 3H), 0.84−0.76 (m, 2H), 0.75−0.66 (m, 2H). ^{13}C NMR (101 MHz, DMSO-d_6) δ 168.25, 156.93, 150.89, 148.20, 145.01, 136.87, 136.41, 134.17, 122.04, 114.96, 114.85, 111.72, 76.34, 74.77, 59.67, 42.84, 32.92, 24.24, 23.30, 6.52. HPLC R_t= 2.093 min in 4 min chromatography, purity 96.6%. LC-MS R_t= 1.136 min in 3 min chromatography, purity 100%, MS ESI calcd. for 446.22 $[M + H]^+$ 447.22, found 447.2.

■ ASSOCIATED CONTENT

Supporting Information

The Supporting Information is available free of charge at https://pubs.acs.org/doi/10.1021/acsomega.3c05377.

SMARTCyp prediction of P450 metabolism of SGC-CK2-1 (**1a**), inhibition of **2h** metabolism by 1-ABT, dose-ranging study of EA tolerability in mice by i.p. dosing, and NMR spectra (PDF)

■ AUTHOR INFORMATION

Corresponding Author

Timothy M. Willson − *Structural Genomics Consortium, UNC Eshelman School of Pharmacy, University of North Carolina at Chapel Hill, Chapel Hill, North Carolina 27599, United States; Rapidly Emerging Antiviral Drug Development Initiative (READDI), Chapel Hill, North Carolina 27599, United States;* orcid.org/0000-0003-4181-8223; Email: tim.willson@unc.edu

Authors

Xuan Yang − *Structural Genomics Consortium, UNC Eshelman School of Pharmacy, University of North Carolina at Chapel Hill, Chapel Hill, North Carolina 27599, United States; Rapidly Emerging Antiviral Drug Development Initiative (READDI), Chapel Hill, North Carolina 27599, United States*

Han Wee Ong − *Structural Genomics Consortium, UNC Eshelman School of Pharmacy, University of North Carolina at Chapel Hill, Chapel Hill, North Carolina 27599, United*

https://doi.org/10.1021/acsomega.3c05377
ACS Omega 2023, 8, 39546−39561

States; Rapidly Emerging Antiviral Drug Development Initiative (READDI), Chapel Hill, North Carolina 27599, United States; orcid.org/0000-0003-3232-2373

Rebekah J. Dickmander − *Rapidly Emerging Antiviral Drug Development Initiative (READDI), Chapel Hill, North Carolina 27599, United States; Department of Microbiology & Immunology, Lineberger Comprehensive Cancer Center, and Department of Chemistry, University of North Carolina at Chapel Hill, Chapel Hill, North Carolina 27599, United States*

Jeffery L. Smith − *Structural Genomics Consortium, UNC Eshelman School of Pharmacy, University of North Carolina at Chapel Hill, Chapel Hill, North Carolina 27599, United States*

Jason W. Brown − *Takeda Development Center Americas, Inc., San Diego, California 92121, United States*

William Tao − *Takeda Development Center Americas, Inc., San Diego, California 92121, United States*

Edcon Chang − *Takeda Development Center Americas, Inc., San Diego, California 92121, United States;* orcid.org/0000-0001-9534-0291

Nathaniel J. Moorman − *Rapidly Emerging Antiviral Drug Development Initiative (READDI), Chapel Hill, North Carolina 27599, United States; Department of Microbiology & Immunology and Lineberger Comprehensive Cancer Center, University of North Carolina at Chapel Hill, Chapel Hill, North Carolina 27599, United States*

Alison D. Axtman − *Structural Genomics Consortium, UNC Eshelman School of Pharmacy, University of North Carolina at Chapel Hill, Chapel Hill, North Carolina 27599, United States; Rapidly Emerging Antiviral Drug Development Initiative (READDI), Chapel Hill, North Carolina 27599, United States;* orcid.org/0000-0003-4779-9932

Complete contact information is available at: https://pubs.acs.org/10.1021/acsomega.3c05377

Author Contributions

T.M.W., A.D.A., and N.J.M. conceived the study. X.Y., H.W.O., J.W.B., W.T., E.C., and A.D.A. designed the experiments and compounds. R.J.D. and J.L.S. performed the biological studies. T.M.W. wrote the manuscript. All authors read and approved the manuscript.

Funding

The Structural Genomics Consortium (SGC) is a registered charity (no. 1097737) that receives funds from Bayer AG, Boehringer Ingelheim, Bristol Myers Squibb, Genentech, Genome Canada through Ontario Genomics Institute [OGI-196], EU/EFPIA/OICR/McGill/KTH/Diamond Innovative Medicines Initiative 2 Joint Undertaking [EUbOPEN grant 875510], Janssen, Merck KGaA (aka EMD in Canada and United States), Pfizer, and Takeda. Research reported in this publication was supported in part by the NC Biotech Center Institutional support grant 2018-IDG-1030, by the NIH Illuminating the Druggable Genome 1U24DK116204-01, and Department of Defense ALSRP award AL190107. This project was supported by the Rapidly Emerging Antiviral Drug Development Initiative (READDI) at the University of North Carolina at Chapel Hill with funding from the North Carolina Coronavirus State and Local Fiscal Recovery Funds program, appropriated by the North Carolina General Assembly. Additional funding was provided by a grant from Millennium Pharmaceuticals (Takeda).

Notes

The authors declare no competing financial interest.

■ ACKNOWLEDGMENTS

Constructs for NanoBRET measurements of CSNK2A1 and CSNK2A2 were provided by Promega Corporation (Madison, WI). We thank K. Saikatendu Singh (Takeda, San Diego, CA) for facilitating collaborative interactions and constructive criticism throughout the project. WuXi AppTec (Shanghai, China) provided the chemical synthesis support. Analiza, Inc. (Cleveland, OH) performed kinetic solubility and mouse liver microsome studies. Pharmaron (Beijing, China) provided the in vitro and in vivo pharmacokinetic assay support.

■ ABBREVIATIONS USED:

CSNK2A, casein kinase **2a**; PZP, 3-cyano-7-cyclopropylamino-pyrazolo[1,5-*a*]pyrimidine; GST, glutathione *S*-transferase; MHV, mouse hepatitis virus; MLM, mouse liver microsome; i.v., intravenous; i.p., intraperitoneal; C_{max}, maximum concentration; AUC, area under the curve; CL_{int}, intrinsic clearance; EA, ethacrynic acid; 1-ABT, 1-aminobenzotriazole

■ REFERENCES

(1) Li, G.; Hilgenfeld, R.; Whitley, R.; De Clercq, E. Therapeutic Strategies for COVID-19: Progress and Lessons Learned. *Nat. Rev. Drug Discovery* **2023**, *22*, 1−27.

(2) Kumar, N.; Sharma, S.; Kumar, R.; Tripathi, B. N.; Barua, S.; Ly, H.; Rouse, B. T. Host-Directed Antiviral Therapy. *Clin. Microbiol. Rev.* **2020**, *33* (3), e00168.

(3) García-Cárceles, J.; Caballero, E.; Gil, C.; Martínez, A. Kinase Inhibitors as Underexplored Antiviral Agents. *J. Med. Chem.* **2022**, *65* (2), 935−954.

(4) Ramón, A. C.; Pérez, G. V.; Caballero, E.; Rosales, M.; Aguilar, D.; Vázquez-Blomquist, D.; Ramos, Y.; Rodríguez-Ulloa, A.; Falcón, V.; Rodríguez-Moltó, M. P.; Yang, K.; Perera, Y.; Perea, S. E. Targeting of Protein Kinase CK2 Elicits Antiviral Activity on Bovine Coronavirus Infection. *Viruses* **2022**, *14* (3), 552.

(5) Yang, X.; Dickmander, R. J.; Bayati, A.; Taft-Benz, S. A.; Smith, J. L.; Wells, C. I.; Madden, E. A.; Brown, J. W.; Lenarcic, E. M.; Yount, B. L., Jr.; Chang, E.; Axtman, A. D.; Baric, R. S.; Heise, M. T.; McPherson, P. S.; Moorman, N. J.; Willson, T. M. Host Kinase CSNK2 is a Target for Inhibition of Pathogenic SARS-like *β*-Coronaviruses. *ACS Chem. Biol.* **2022**, *17* (7), 1937−1950.

(6) Quezada Meza, C. P.; Ruzzene, M. Protein Kinase CK2 and SARS-CoV-2: An Expected Interplay Story. *Kinases Phosphatases* **2023**, *1* (2), 141−150.

(7) Dowling, J. E.; Chuaqui, C.; Pontz, T. W.; Lyne, P. D.; Larsen, N. A.; Block, M. H.; Chen, H.; Su, N.; Wu, A.; Russell, D.; Pollard, H.; Lee, J. W.; Peng, B.; Thakur, K.; Ye, Q.; Zhang, T.; Brassil, P.; Racicot, V.; Bao, L.; Denz, C. R.; Cooke, E. Potent and Selective Inhibitors of CK2 Kinase Identified through Structure-Guided Hybridization. *ACS Med. Chem. Lett.* **2012**, *3* (4), 278−283.

(8) Wells, C. I.; Drewry, D. H.; Pickett, J. E.; Tjaden, A.; Krämer, A.; Müller, S.; Gyenis, L.; Menyhart, D.; Litchfield, D. W.; Knapp, S.; Axtman, A. D. Development of a Potent and Selective Chemical Probe for the Pleiotropic Kinase CK2. *Cell Chem. Biol.* **2021**, *28* (4), 546−558.

(9) Dowling, J. E.; Alimzhanov, M.; Bao, L.; Block, M. H.; Chuaqui, C.; Cooke, E. L.; Denz, C. R.; Hird, A.; Huang, S.; Larsen, N. A.; Peng, B.; Pontz, T. W.; Rivard-Costa, C.; Saeh, J. C.; Thakur, K.; Ye, Q.; Zhang, T.; Lyne, P. D. Structure and Property Based Design of Pyrazolo[1,5-a]pyrimidine Inhibitors of CK2 Kinase with Activity in Vivo. *ACS Med. Chem. Lett.* **2013**, *4* (8), 800−805.

(10) Dowling, J. E.; Alimzhanov, M.; Bao, L.; Chuaqui, C.; Denz, C. R.; Jenkins, E.; Larsen, N. A.; Lyne, P. D.; Pontz, T.; Ye, Q.; Holdgate, G. A.; Snow, L.; O'Connell, N.; Ferguson, A. D. Potent and Selective

CK2 Kinase Inhibitors with Effects on Wnt Pathway Signaling in Vivo. *ACS Med. Chem. Lett.* **2016**, *7* (3), 300−305.
(11) Dinnon, K. H., 3rd; Leist, S. R.; Schäfer, A.; Edwards, C. E.; Martinez, D. R.; Montgomery, S. A.; West, A.; Yount, B. L., Jr.; Hou, Y. J.; Adams, L. E.; Gully, K. L.; Brown, A. J.; Huang, E.; Bryant, M. D.; Choong, I. C.; Glenn, J. S.; Gralinski, L. E.; Sheahan, T. P.; Baric, R. S. A Mouse-adapted Model of SARS-CoV-2 to Test COVID-19 Countermeasures. *Nature* **2020**, *586* (7830), 560−566.
(12) Leist, S. R.; Dinnon, K. H., 3rd; Schäfer, A.; Tse, L. V.; Okuda, K.; Hou, Y. J.; West, A.; Edwards, C. E.; Sanders, W.; Fritch, E. J.; Gully, K. L.; Scobey, T.; Brown, A. J.; Sheahan, T. P.; Moorman, N. J.; Boucher, R. C.; Gralinski, L. E.; Montgomery, S. A.; Baric, R. S. A Mouse-Adapted SARS-CoV-2 Induces Acute Lung Injury and Mortality in Standard Laboratory Mice. *Cell* **2020**, *183* (4), 1070−1085.
(13) Rydberg, P.; Gloriam, D. E.; Olsen, L. The SMARTCyp Cytochrome P450 Metabolism Prediction Server. *Bioinformatics* **2010**, *26* (23), 2988−2989.
(14) Rydberg, P.; Gloriam, D. E.; Zaretzki, J.; Breneman, C.; Olsen, L. SMARTCyp: A 2D Method for Prediction of Cytochrome P450-Mediated Drug Metabolism. *ACS Med. Chem. Lett.* **2010**, *1* (3), 96−100.
(15) Tyzack, J. D.; Kirchmair, J. Computational Methods and Tools to Predict Cytochrome P450 Metabolism for Drug Discovery. *Chem. Biol. Drug Des.* **2019**, *93* (4), 377−386.
(16) Lewis, D. F. V.; Dickins, M. Baseline Lipophilicity Relationships in Human Cytochromes P450 Associated with Drug Metabolism. *Drug Metab. Rev.* **2003**, *35* (1), 1−18.
(17) Di, L.; Keefer, C.; Scott, D. O.; Strelevitz, T. J.; Chang, G.; Bi, Y. A.; Lai, Y.; Duckworth, J.; Fenner, K.; Troutman, M. D.; Obach, R. S. Mechanistic Insights from Comparing Intrinsic Clearance Values Between Human Liver Microsomes and Hepatocytes to Guide Drug Design. *Eur. J. Med. Chem.* **2012**, *57*, 441−448.
(18) Potęga, A. Glutathione-Mediated Conjugation of Anticancer Drugs: An Overview of Reaction Mechanisms and Biological Significance for Drug Detoxification and Bioactivation. *Molecules* **2022**, *27* (16), 5252.
(19) Driscoll, J. P.; Yadav, A. S.; Shah, N. R. Role of Glucuronidation and P450 Oxidation in the Bioactivation of Bromfenac. *Chem. Res. Toxicol.* **2018**, *31* (4), 223−230.
(20) MacFaul, P. A.; Morley, A. D.; Crawford, J. J. A Simple In Vitro Assay for Assessing the Reactivity of Nitrile Containing Compounds. *Bioorg. Med. Chem. Lett.* **2009**, *19* (4), 1136.
(21) Oakley, A. Glutathione Transferases: a Structural Perspective. *Drug Metab. Rev.* **2011**, *43* (2), 138.
(22) Allocati, N.; Masulli, M.; Di Ilio, C.; Federici, L. Glutathione Transferases: Substrates, Inihibitors and Pro-drugs in Cancer and Neurodegenerative Diseases. *Oncogenesis* **2018**, *7* (1), 8.
(23) Ploemen, J. H. T. M.; Ommen, B. V.; Bogaards, J. J. P.; Van Bladeren, P. J. Ethacrynic Acid and its Glutathione Conjugate as Inhibitors of Glutathione S-transferases. *Xenobiotica* **1993**, *23* (8), 913−923.
(24) Townsend, D. M.; Tew, K. D. The Role of Glutathione-S-transferase in Anti-cancer Drug Resistance. *Oncogene* **2003**, *22* (47), 7369−7375.
(25) Kim, Y.; Gast, S. M.; Endo, T.; Lu, D.; Carson, D.; Schmidt-Wolf, I. G. H. In Vivo Efficacy of the Diuretic Agent Ethacrynic Acid Against Multiple Myeloma. *Leuk. Res.* **2012**, *36* (5), 598−600.
(26) Liu, B.; Huang, X.; Hu, Y.; Chen, T.; Peng, B.; Gao, N.; Jin, Z.; Jia, T.; Zhang, N.; Wang, Z.; Jin, G. Ethacrynic Acid Improves the Antitumor Effects of Irreversible Epidermal Growth Factor Receptor Tyrosine Kinase Inhibitors in Breast Cancer. *Oncotarget* **2016**, *7* (36), 58038−58050.
(27) Schmidt, M.; Kim, Y.; Gast, S. M.; Endo, T.; Lu, D.; Carson, D.; Schmidt-Wolf, I. G. H. Increased In Vivo Efficacy of Lenalidomide and Thalidomide by Addition of Ethacrynic Acid. *In Vivo* **2011**, *25* (3), 325−333.
(28) de Montellano, P. R. O. 1-Aminobenzotriazole: A Mechanism-Based Cytochrome P450 Inhibitor and Probe of Cytochrome P450 Biology. *Med. Chem.* **2018**, *8* (3), 038−065.
(29) Salvi, M.; Borgo, C.; Pinna, L. A.; Ruzzene, M. Targeting CK2 in Cancer: a Valuable Strategy or a Waste of Time? *Cell Death Discovery* **2021**, *7* (1), 325.
(30) Pack, M.; Gotz, C.; Wrublewsky, S.; Montenarh, M. SGC-CK2-1 Is an Efficient Inducer of Insulin Production and Secretion in Pancreatic β-Cells. *Pharmaceutics* **2021**, *14* (1), 19.
(31) Boewe, A. S.; Wemmert, S.; Kulas, P.; Schick, B.; Gotz, C.; Wrublewsky, S.; Montenarh, M.; Menger, M. D.; Laschke, M. W.; Ampofo, E. Inhibition of CK2 Reduces NG2 Expression in Juvenile Angiofibroma. *Biomedicines* **2022**, *10* (5), 966.
(32) Mishra, S.; Kinoshita, C.; Axtman, A. D.; Young, J. E. Evaluation of a Selective Chemical Probe Validates That CK2Mediates Neuroinflammation in a Human Induced Pluripotent Stem Cell-Derived Mircroglial Model. *Front. Mol. Neurosci.* **2022**, *15*, No. 824956.
(33) Al Shoyaib, A.; Archie, S. R.; Karamyan, V. T. Intraperitoneal Route of Drug Administration: Should it Be Used in Experimental Animal Studies? *Pharm. Res.* **2019**, *37* (1), 12.
(34) Cannon, P. J.; Heinemann, H. O.; Stason, W. B.; Laragh, J. H. Ethacrynic Acid: Effectiveness and Mode of Diuretic Action in Man. *Circulation* **1965**, *31*, 5−18.

https://doi.org/10.1021/acsomega.3c05377
ACS Omega 2023, 8, 39546−39561